Caveolin gene transfer improves glucose metabolism in diabetic mice

Koji Otsu, Yoshiyuki Toya, Jin Oshikawa, Reiko Kurotani, Takuya Yazawa, Motohiko Sato, Utako Yokoyama, Satoshi Umemura, Susumu Minamisawa, Satoshi Okumura and Yoshihiro Ishikawa

Am J Physiol Cell Physiol 298:C450-C456, 2010. First published 18 November 2009; doi:10.1152/ajpcell.00077.2009

Am J Physiol Cell Physiol 298: C450–C456, 2010.
First published November 18, 2009; doi:10.1152/ajpcell.00077.2009.

Caveolin gene transfer improves glucose metabolism in diabetic mice

Koji Otsu,[1] Yoshiyuki Toya,[2] Jin Oshikawa,[2] Reiko Kurotani,[1] Takuya Yazawa,[3] Motohiko Sato,[1] Utako Yokoyama,[1] Satoshi Umemura,[2] Susumu Minamisawa,[1,4] Satoshi Okumura,[1] and Yoshihiro Ishikawa[1,5]

[1]*Cardiovascular Research Institute,* [2]*Department of Cardiorenal Medicine, and* [3]*Department of Pathobiology, Yokohama City University Graduate School of Medicine, Yokohama, Japan;* [4]*Consolidated Research Institute for Advanced Science and Medical Care, Waseda University, Tokyo, Japan; and* [5]*Cardiovascular Research Institute, Departments of Cell Biology and Molecular Medicine and Medicine (Cardiology), New Jersey Medical School, Newark, New Jersey*

Submitted 9 March 2009; accepted in final form 4 November 2009

Otsu K, Toya Y, Oshikawa J, Kurotani R, Yazawa T, Sato M, Yokoyama U, Umemura S, Minamisawa S, Okumura S, Ishikawa Y. Caveolin gene transfer improves glucose metabolism in diabetic mice. *Am J Physiol Cell Physiol* 298: C450–C456, 2010. First published November 18, 2009; doi:10.1152/ajpcell.00077.2009.— Caveolin, a member of the membrane-anchoring protein family, accumulates various growth receptors in caveolae and inhibits their function. Upregulation of caveolin attenuates cellular proliferation and growth. However, the role of caveolin in regulating insulin signals remains controversial. Here, we demonstrate that caveolin potently enhances insulin receptor (IR) signaling when overexpressed in the liver in vivo. Adenovirus-mediated gene transfer was used to overexpress caveolin specifically in the liver of diabetic obese mice, which were generated with a high-fat diet. Expression of molecules involved in IR signaling, such as IR or Akt, remained unchanged after gene transfer. However, hepatic glycogen synthesis was markedly increased with a decrease in phosphoenolpyruvate carboxykinase protein expression. Insulin sensitivity was increased after caveolin gene transfer as determined by decreased blood glucose levels in response to insulin injection and fasting blood glucose levels. Glucose tolerant test performance was also improved. Similar improvements were obtained in *KKA^y* genetically diabetic mice. Adenovirus-mediated overexpression of caveolin-3 in hepatic cells also enhanced IR signaling, as shown by increased phosphorylation of IR in response to insulin stimulation and higher glycogen synthesis at baseline. These effects were attributed mostly to increased insulin receptor activity and caveolin-mediated, direct inhibition of protein tyrosine phosphatase 1B, which was increased in obese mouse livers. In conclusion, our results suggest that caveolin is an important regulator of glucose metabolism that can enhance insulin signals.

insulin receptor; diabetes mellitus

CAVEOLIN (CAV) IS COMPOSED of three subtypes (Cav1, Cav2, and Cav3), and it is a major protein component of caveolae, which are flask-shaped, cell membrane invaginations that are abundantly expressed in adipocytes, myocytes, and endothelial cells (5). Caveolae accumulate multiple receptors and kinases that are involved in cell growth and proliferation (11, 19). The net effect of these interactions is the suppression of cellular growth and proliferation signals (5). Accordingly, it is widely believed that Cav is a potent growth suppressor.

Despite numerous studies demonstrating an important role for Cav in regulating various growth signals, the role of Cav in regulating insulin receptor (IR) signals has remained rather controversial. Some studies have shown a positive association of Cav with IR signals (3, 22) while others have refuted these findings (10). Nevertheless, it has been proposed that Cav may not inhibit insulin signals, but may be required or even activate this signaling pathway (28). Mice with a disrupted Cav1 gene, which is most abundantly expressed in adipocytes, showed decreased IR protein expression and developed insulin resistance in fat tissues (7). Similarly, mice with disrupted Cav3, which is abundantly expressed in the muscles (9), developed insulin resistance in the skeletal muscles (22). Furthermore, a previous study used purified proteins to demonstrate that a small peptide derived from Cav stimulated IR kinase activity in vitro; interestingly, this stimulation was more potent with a peptide derived from Cav3 than Cav1 (30). These findings have suggested that Cav plays an important role in maintaining physiological insulin signals in the major target organs of insulin action, i.e., the liver and fat tissues.

In the present study, we have addressed the role of Cav in the liver. The liver is a major insulin target that expresses only a small amount of endogenous Cav, suggesting that the liver, unlike fat tissues and skeletal muscles, does not require high Cav levels, at least, under normal conditions. We have examined the effect of Cav3 gene transfer to the livers of diabetic obese mice fed a high-fat diet or *KKA^y* mice, a widely used Type 2 diabetic model (17). We demonstrated that Cav enhances IR signaling in vivo and in vitro. Insulin sensitivity and thus glucose metabolism were markedly improved by Cav3 gene transfer in diabetic mice, as exemplified by increased hepatic glycogen synthesis and improved glucose tolerance test performance.

MATERIALS AND METHODS

Diabetic mouse models. At weaning, mice (3 wk of age) were placed on either a high-fat diet (59% of calories derived from fat) for diabetic obese mice or a normal chow diet (10% of calories derived from fat) for lean normal mice (Oriental Yeast, Tokyo, Japan) for at least 6 mo. Differences in body weight became significant at 5 wk (Fig. 1*A*). At 6 mo, fasting blood glucose (FBG) levels were increased approximately threefold (Fig. 1*B*) and serum triglycerides by 20% (Fig. 1*C*) in obese diabetic mice relative to lean normal mice.

KKA^y mice were purchased from CLEA Japan (Tokyo, Japan) and used for experiments at 10 wk old. All animals were maintained in accordance with the guidelines of the animal experiment committees of Yokohama City University, and experiments were approved by the Ethical Committee of Animal Experiments of Yokohama City University School of Medicine.

Adenovirus construction and injection into mice. Full-length cDNA encoding rat Cav3 was cloned into the shuttle vector to construct an adenoviral vector harboring Cav3 or green fluorescent protein (GFP; control) using an AdenoX adenovirus construction kit (Clontech, Palo

Address for reprint requests and other correspondence: Y. Ishikawa, Cardiovascular Research Institute, Yokohama City University Graduate School of Medicine 3-9 Fukuura, Kanazawa-ku, Yokohama 236-0004, Japan.

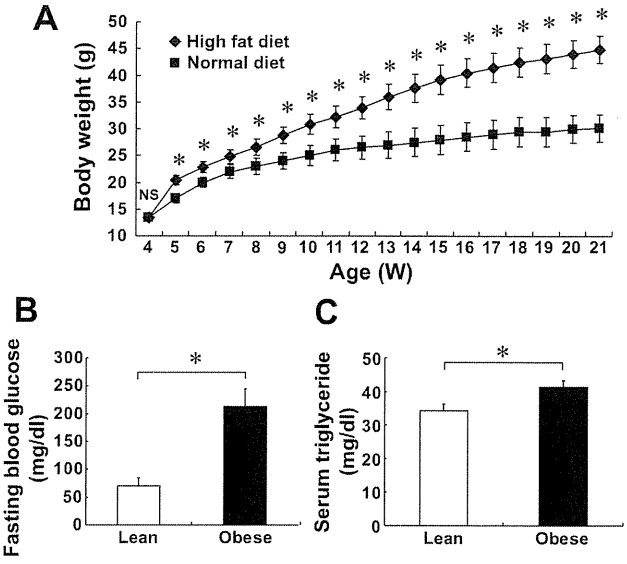

Fig. 1. Generation of obese diabetic mice. *A*: changes in body weight between obese mice and age (W, weeks)-matched, normal lean mice ($n = 31$, $^*P < 0.05$; NS, not significant). *B* and *C*: comparison of fasting blood glucose levels ($n = 8$–13, $^*P < 0.05$) (*B*) and serum triglycerides ($n = 4$–5, $^*P < 0.05$) (*C*) between lean control (Lean) and obese diabetic (Obese) mice.

Alto, CA) (11). An adenovirus titer of 1.0×10^7 plaque-forming units (PFU) was sufficient to overexpress Cav3 in the liver to levels equivalent to endogenous Cav3 in the skeletal muscles, where Cav3 is most abundantly expressed, for up to 6 days after viral injection (Fig. 2, *A* and *B*).

Radioligand binding assays and Western blot analysis. Radioligand binding assays for cell surface IR were performed using HepG2 cells and ^{125}I-labeled insulin as previously described (20, 24). Immunoblotting of Cav, IR-β, and its related molecules was performed as previously described (21, 22).

Immunoprecipitation assays. An in vivo phosphorylation assay for IR-β or insulin receptor substrate (IRS) was performed as previously described (22). After anesthesia was induced with pentobarbital sodium intraperitoneally (100 mg/kg ip), tissues were quickly harvested and stored in liquid nitrogen. Immunoprecipitation of Cav, IR-β, and its related molecules was performed as we previously described (22).

Protein fractionation by the sucrose gradient method. Caveolae fractions were separated by the sodium carbonate-based, detergent-free method (26, 30).

Glucose and insulin tolerance tests. After a 16-h period of fasting, glucose (2 mg/g body wt ip) was injected. FBG levels were determined at 0, 30, 60, 90, and 120 min after injection using a glucometer (22). For the insulin tolerance test, insulin was injected (0.75 U/kg ip), and then FBG levels were measured (7).

Measurements of hepatic glycogen synthesis and triglycerides. Glycogen was measured as previously described (27). Briefly, livers were homogenized in 6 M perchloric acid. The homogenate was boiled for 5 min at 100°C and centrifuged at 10,000 *g*. Glycogen in the supernatant was precipitated with ethanol and measured by a phenol-sulfuric acid reaction. Hepatic triglycerides were extracted as described previously (13). Briefly, tissues were homogenized in extraction buffer (20 mM Tris, pH 7.3, 1 mM EDTA, and 1 mM β-mercaptoethanol), after which chloroform, methanol, and water were added. The mixture was centrifuged at 3,000 *g*. The lower phase was evaporated and redissolved in isopropanol, and triglyceride concentrations were determined with the GPO-Trinder (Sigma, St. Louis, MO).

Measurements of serum lipids. Total cholesterol and triglycerides were determined as we described previously (22).

Cell culture. HepG2 cells, a human hepatocellular carcinoma cell line, were cultured in Dulbecco's modified Eagle's medium containing 5% fetal bovine serum and 10% horse serum in a humidified 95% air-5% CO_2 incubator.

Inhibition of phosphatase activity by Cav peptides. Phosphatase activity was measured colorimetrically using a commercial assay kit (Calbiochem, San Diego, CA) and purified protein tyrosine phosphatase 1B (PTP1B) (Upstate, Lake Placid, NY) in the presence or absence of the following Cav peptides; for the scaffolding domain

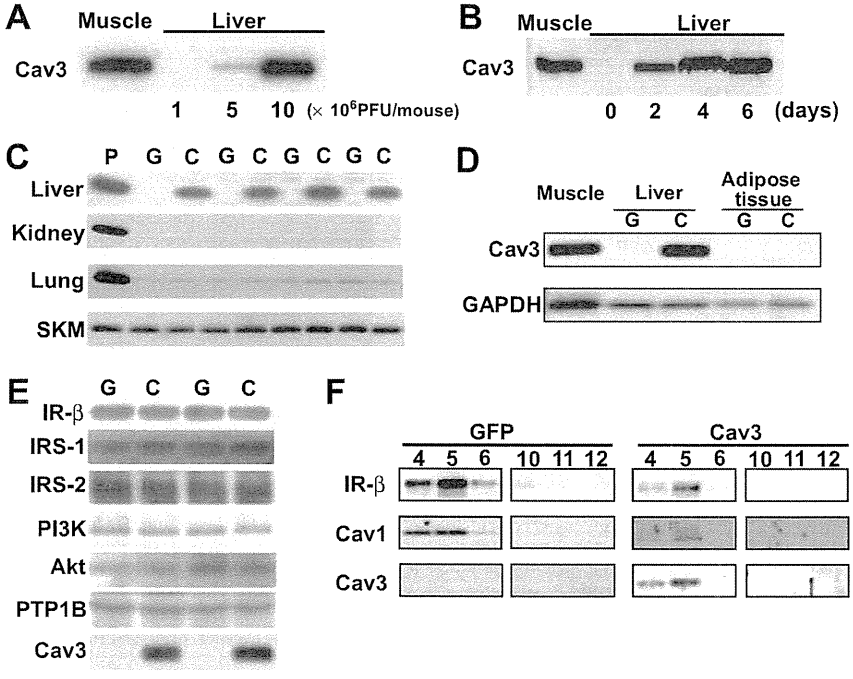

Fig. 2. Caveolin-3 (Cav3) gene transfer to the liver. Adenovirus harboring the Cav3 or green fluorescent protein (GFP) gene was injected into the tail veins of mice. *A*: dose-dependent Cav3 expression in whole liver homogenates. Adenovirus harboring the Cav3 or GFP (control) gene was injected at 0, 1, 5, or 10×10^6 plaque-forming units (PFU). An equivalent amount of total protein from muscle samples was used as positive control (*left lane*). *B*: time-dependent Cav3 expression in the liver. Livers were harvested at 2, 4, and 6 days after injection and analyzed by immunoblotting. *C*: Cav3 expression in various organs of mice after Cav3 gene transfer (C) vs. GFP gene transfer (G). Cav3 protein expression was detected only in the liver. Muscle was used as positive control (P). SKM, skeletal muscle. *D*: Cav3 expression after Cav3 gene transfer in adipose tissues. GAPDH is shown as loading standard. *E*: expression of molecules involved in insulin receptor (IR) signaling in hepatic tissues after Cav3 or GFP gene transfer. IRS-1 and 2, insulin receptor substrate 1 and 2; PTP1B, protein tyrosine phosphatase 1B; PI3K, phosphatidylinositol 3-kinase. *F*: sucrose gradient fractionation of liver proteins and immunoblotting of exogenous Cav3, endogenous Cav1, and IR-β (*lanes 4, 5,* and *6*, caveolar fractions; *lanes 10, 11,* and *12*, noncaveolar fractions)

(SD) peptide: Cav3 (SD-Cav3)-DGVWRVSYTTFTVSKYWCYR; Cav1 (SD-Cav1)-DGIWKASFTTFTVTKYWFYR; for the nonscaffolding domain (NSD) peptide: Cav3 (NSD-Cav3)-NRDPKNINEDIVKVDFEDVIAEPEG; Cav1 (NSD-Cav1)-NRDPKHLNDDVVKIDFEDVIAEPEG. Briefly, purified PTP1B (0.022 units) was incubated with increasing concentrations of Cav peptide (0, 0.63, 1.25, 2.5, 5, and 10 μM) at room temperature for 10 min, followed by the addition of the enzyme substrate and an additional 15-min incubation. PTP1B activity was determined by spectrophotometry.

RESULTS

Overexpression of Cav3 in the liver. The liver expressed relatively small amounts of endogenous Cav1, and little Cav3 was detected by immunoblotting mouse liver homogenates. Using the Cav3 adenovirus (1.0×10^7 PFU), Cav3 expression in liver homogenates was comparable to that of endogenous Cav3 in the skeletal muscle (Fig. 2*A*), another major organ involved in regulating glucose metabolism that abundantly expresses Cav. With this amount of adenovirus, the expression of Cav3 peaked at *day 4* postinjection and plateaued at least until *day 6* (Fig. 2*B*). The gene delivery of Cav3 was restricted to the liver, and there was no increase in Cav3 expression in the other organs such as skeletal muscles or adipose tissues (Fig. 2, *C* and *D*). Despite Cav3 overexpression, the protein expression of IR-β as well as other molecules involved in IR signaling such as IRS, phosphatidylinositol 3-kinase (PI3K), Akt, or PTP1B were unchanged (Fig. 2*E*), suggesting that Cav3 does not regulate the protein expression of these molecules, at least, in the liver. The subcellular distribution of exogenous Cav3 and endogenous IR-β, as determined by sucrose gradient fractionation of liver tissues, was unchanged and similar to that of endogenous Cav1 (Fig. 2*F*), and insulin binding assays using intact hepatic cells revealed no changes in B_{max} [GFP vs. Cav3: 4.2 ± 0.1 vs. 4.3 ± 0.2, $n = 4$, P = not significant (NS)] or K_d (GFP vs. Cav3: 58.4 ± 0.1 vs. 58.9 ± 0.4 fmol, $n = 4$, P = NS) with Cav3 gene transfer, suggesting that Cav3 gene transfer did not alter the caveolar and/or the cell surface localization of IR.

Cav3 gene transfer is associated with increased glycogen synthesis in the liver. Because one of the most important actions of insulin is to promote glycogen synthesis in tissues (23), we examined whether Cav3 gene transfer changed the glycogen content in the livers of diabetic obese mice and found that it was significantly increased in mice with Cav3 gene transfer (Fig. 3*A*). Fat deposition was similar in the livers of diabetic obese mice with Cav3 gene transfer and GFP gene transfer, indicating that it was caused by a high-fat diet and not by Cav3 overexpression. The increase in glycogen content in mice with Cav3 gene transfer was accompanied by a decrease in protein expression of the cytosolic form of phosphoenolpyruvate carboxykinase (PEPCK) (Fig. 3*C*). This enzyme catalyzes the first irreversible reaction in gluconeogenesis, and the activity of PEPCK is proportional to the amount of this

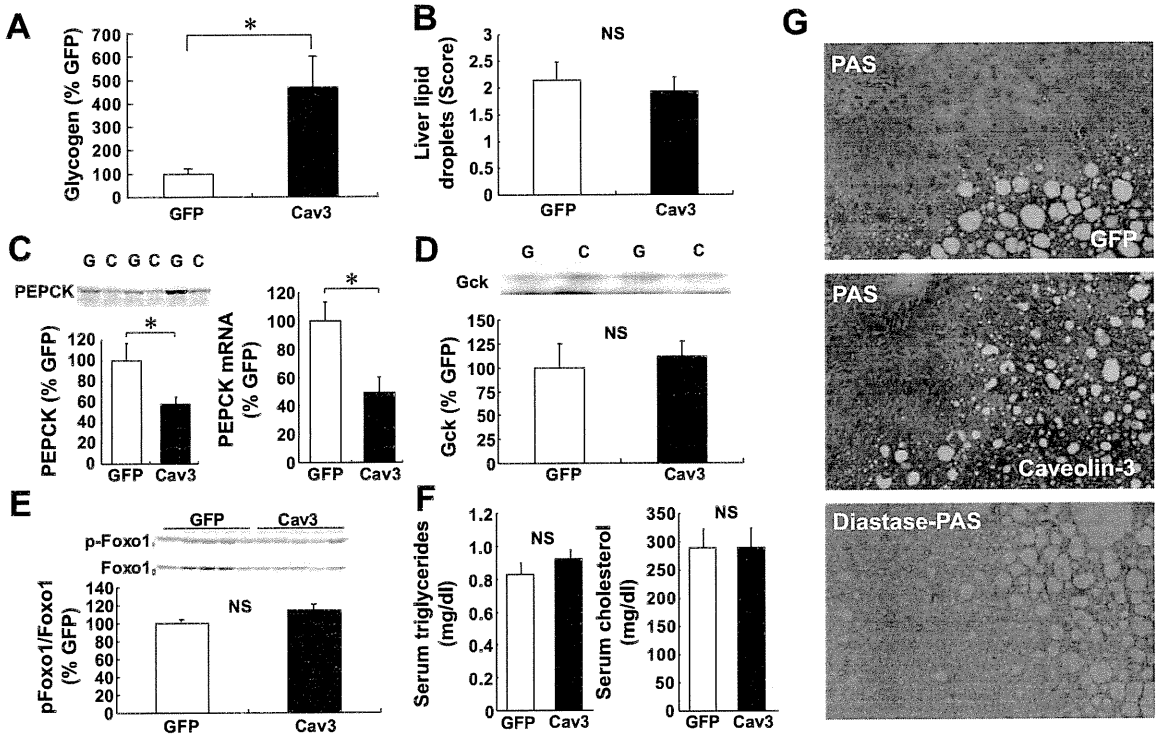

Fig. 3. Increased glycogen content in the liver after Cav gene transfer. *A*: hepatic glycogen content at baseline after Cav3 vs. GFP gene transfer in diabetic obese mice ($n = 4$, $^*P < 0.05$). *B*: hepatic lipid droplet score comparison after Cav3 vs. GFP gene transfer ($n = 7$–8; NS, not significant). *C*: hepatic phosphoenolpyruvate carboxykinase (PEPCK) expression by immunoblotting and quantitative RT-PCR. A representative immunoblot is shown in the *inset* ($n = 4$–5, $^*P < 0.05$). *D*: glucokinase expression by immunoblotting ($n = 4$, NS). *E*: activation of Foxo1 transcriptional factor ($n = 5$, NS). *F*: serum lipid concentrations after Cav3 gene transfer vs. GFP gene transfer in diabetic obese mice (*left*, triglycerides; *right*, cholesterol) ($n = 4$, NS). *G*: histological examination of hepatic tissues. PAS, periodic acid Schiff (PAS) staining of hepatic tissues from mice after Cav3 or GFP gene transfer; diastase-PAS, PAS staining pretreated with diastase.

enzyme, which is regulated by insulin (15). These findings agree with the concept that insulin signals were enhanced in the liver after Cav3 gene transfer. In contrast, the expression of glucokinase (Gck) and Foxo1 activity remained changed (Fig. 3, *D* and *E*).

Abnormal serum lipid concentrations were not improved, potentially because the duration of Cav3 overexpression was short (Fig. 3*F*). Liver triglycerides and serum leptin concentrations were also unchanged (data not shown). Histology and periodic acid-Schiff (PAS) staining demonstrated that the purple staining of glycogen was greater in mice with Cav3 gene transfer (Fig. 3*G*). There was no staining of glycogen when tissues were pretreated with diastase. We also performed oil red O staining and scored the degree of lipid accumulation in hepatic tissues (16). However, there was no significant difference in the lipid score between GFP and Cav3 groups (GFP 1.94 ± 0.34, Cav3 = 2.14 ± 0.25, $n = 7$–8, P = NS) (Fig. 3*B*).

Similarly, the expression of enzymes involved in lipogenic-related enzymes, such as fatty acid synthase (FAS), sterol regulatory element-binding protein-1, phosphodiesterase 3B, acetyl CoA carboxylase, and liver X receptor, was not significantly different between GFP and Cav3 groups (data not shown).

Cav3 gene transfer improved insulin signals in diabetic obese mice. Cav3 gene injection into diabetic obese mice not only increased the hepatic glycogen content but also improved impaired glucose metabolism. Although Cav3 gene transfer did not alter food intake or body weight (data not shown), impaired glucose tolerance test performance as well as FBG levels (GFP vs. Cav3: 213.3 ± 11.2 vs. 175.3 ± 5.5 mg/dl, $n = 8$, $P <$ 0.05) were significantly improved (Fig. 4*A*). There was no significant difference in glucose tolerance test performance between non-gene and GFP gene-transferred diabetic obese mice (data not shown). This improvement in glucose metabolism was most likely due to increased insulin action as demonstrated by the improved insulin tolerance test performance (Fig. 4*B*). FBG levels remained lower in mice with Cav3 gene transfer than in control mice with GFP gene transfer, even 90 min after insulin challenge. During the glucose tolerance test, insulin levels were not changed by Cav3 gene transfer (Fig. 4*C*)

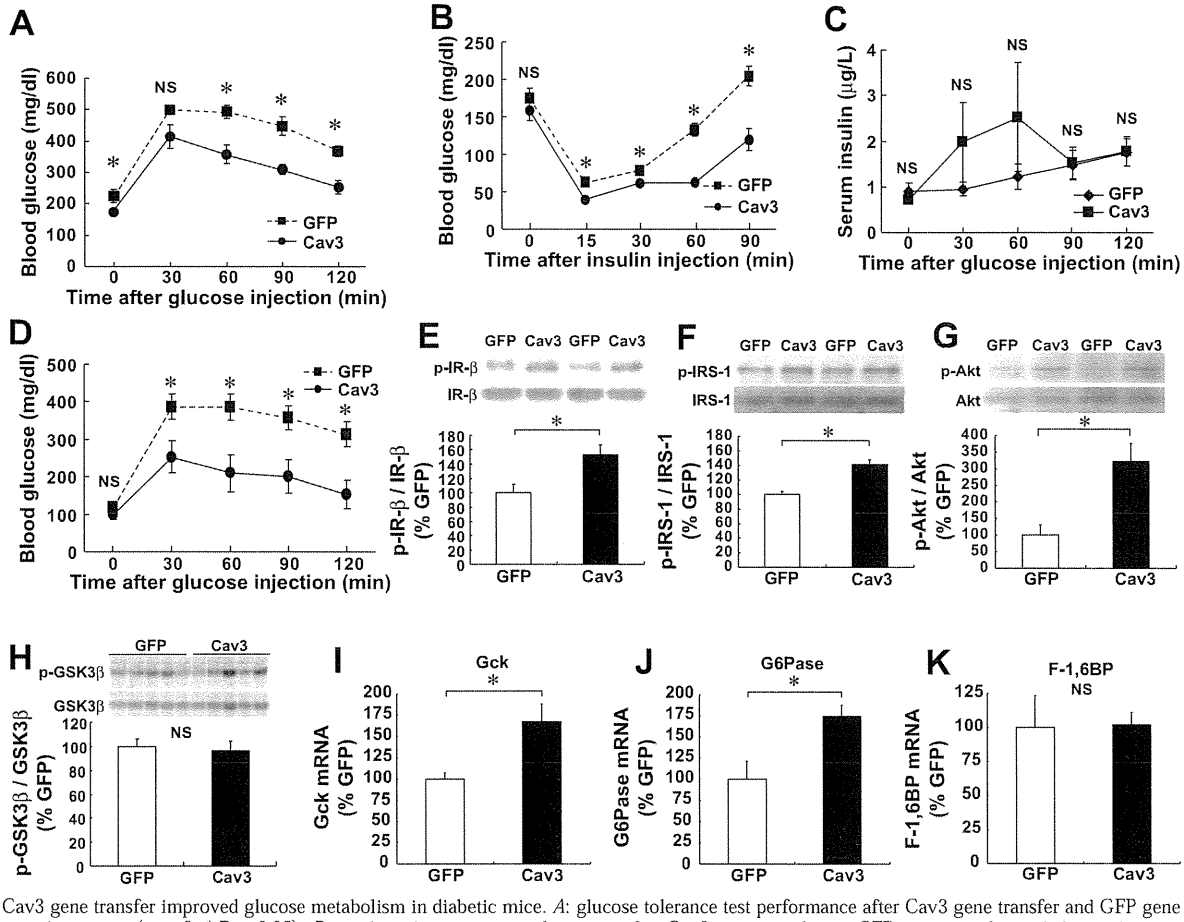

Fig. 4. Cav3 gene transfer improved glucose metabolism in diabetic mice. *A*: glucose tolerance test performance after Cav3 gene transfer and GFP gene transfer in diabetic obese mice ($n = 8$, $^*P < 0.05$). *B*: insulin tolerance test performance after Cav3 gene transfer vs. GFP gene transfer in diabetic obese mice ($n =$ 4, $^*P < 0.05$). *C*: changes in insulin levels during glucose tolerance test ($n = 5$, NS). *D*: glucose tolerance test performance in *KKA*^{y} mice ($n = 4$, $^*P < 0.05$). *E*–*G*: changes in tissue insulin receptor signals after Cav3 gene transfer. Activation of the molecules involved in insulin receptor signaling, IR-β (*E*), IRS-1 (*F*), and Akt (*G*), after Cav3 gene transfer vs. GFP gene transfer in diabetic obese mice. Representative immunoblots are shown in the *insets* ($n = 4$–5, $^*P < 0.05$). *H*: changes in GSK3β activity ($n = 5$, NS). *I*–*K*: mRNA expression of glucose metabolism-related enzyme in mice liver. Glucokinase (Gck; $n = 4$–5, $^*P <$ 0.05), G6Pase ($n = 4$–5, $^*P < 0.05$), and F-1,6BP ($n = 4$–5, NS).

KKA^y mice, which have been widely used as a model of Type 2 diabetes (17), showed only a mild increase in fasting blood glucose concentrations (2), but a marked impairment in glucose tolerance test performance. However, when we injected the Cav3 gene into this mouse model, glucose tolerance test performance was significantly improved (Fig. 4*D*). Therefore, the effect of Cav3 gene transfer on insulin signaling occurs in multiple diabetic mouse models.

Changes in hepatic tissue insulin signaling after Cav3 gene transfer. When whole homogenates of livers from diabetic obese mice with Cav3 gene transfer were examined, we found that IR-β, IRS, and Akt phosphorylation was increased (Fig. 4, *E–G*), suggesting that IR signaling increased after Cav3 gene transfer compared with GFP gene transfer. Because the total protein levels of these molecules including IR-β were not increased, this effect was most likely due to the increased activity of IR-β itself. Because Cav3 gene transfer was restricted to the liver, it was also likely that hepatic Cav3 enhanced the response to insulin, leading to an overall improvement in whole body glucose metabolism. We also examined other relevant enzymes such as Gck, G6Pase, and F-1,6BP (Fig. 4, *I–K*). The mRNA expression of Gck and G6Pase were increased in Cav3 group, suggesting transcriptional activation of these enzymes, while that of F-1,6BP was not changed. The activation of GSK3β was not changed either (Fig. 4*H*).

Cav3 overexpression in hepatic cells. A similar enhancement in insulin signaling by Cav was observed in HepG2 cells, a cultured hepatic cell line. Two days after gene transfer, Cav3 was overexpressed in HepG2 cells to levels equivalent to that of endogenous Cav3 in skeletal muscles (data not shown). IR-β and IRS-1 phosphorylation was significantly enhanced at baseline, which was further increased with increasing concentrations of insulin (0–100 nM) (Fig. 5, *A* and *B*). The maximal activation of IRS-1 was significantly greater in Cav3 gene-transferred cells, suggesting that IR kinase activity in response to insulin was increased by Cav3 overexpression, which confirmed our in vivo observations. At high concentrations (>10 nM), IR-β phosphorylation appeared saturated, while IRS-1 activation was further enhanced in a dose-dependent manner. The cellular content of glycogen was also increased at baseline (Fig. 5*C*). We also examined the phosphorylation of insulin-like growth factor receptors (IGF-1R) in mice with Cav3 gene transfer because IR-β and IGF-1R are structurally similar and Cav3 may alter IGF-1R signaling (14). However, the degree of IGF-1R phosphorylation was similar, suggesting that Cav3 specifically enhances IR-β (Fig. 5*D*).

Caveolin-mediated inhibition of PTP1B activity. The activation of other downstream molecules such as extracellular signal-related kinase (ERK) and phosphatase and tensin homolog (PTEN) in the liver was not significantly different between mice that received Cav3 gene transfer and GFP gene transfer (data not shown). In contrast, it is known that phosphatases, such as PTP1B, can also potently regulate the activity of IR signals (8). In addition, previous studies have demonstrated that PTP1B is present in caveolae (22, 30) and physically interacts with Cav (6). We found that the expression of hepatic PTP1B was significantly increased in diabetic obese mice (Fig. 6*A*) and that overexpressed Cav3 coimmunoprecipitated with PTP1B in the liver (Fig. 6*B*). Furthermore, we found that Cav3 inhibited the activity of PTP1B. A SD-Cav3 peptide, which is known to mimic Cav3 (26), inhibited the activity of purified PTP1B in a dose-dependent manner in vitro, while a similar peptide derived from non-SD Cav3 had no effect (Fig. 6*C*). We also found that a peptide from SD-Cav1 similarly inhibited the activity of PTP1B activity while a NSD-Cav1 had no effect (Fig. 6*D*). These results suggest that Cav3 as well as Cav1 directly interacts with and inhibits the activity of PTP1B. Furthermore, this inhibition may be potentiated in the livers of obese mice where PTP1B expression was increased.

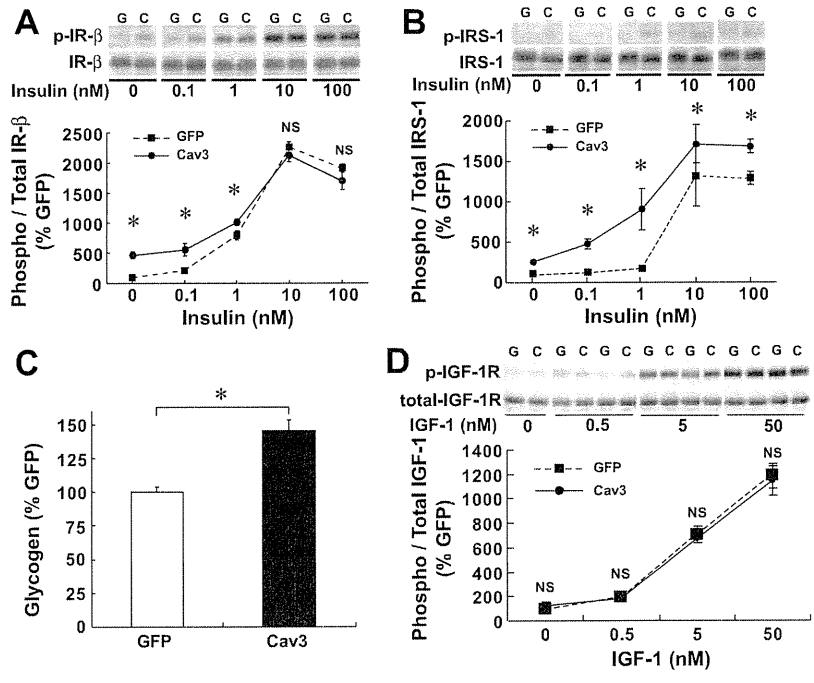

Fig. 5. Cav3 overexpression in HepG2 cells. *A* and *B*: activation of IR-β (*A*) and IRS-1 (*B*) in response to insulin stimulation for 5 min ($n = 5$, $^*P < 0.05$) after Cav3 gene transfer vs. GFP gene transfer. *C*: hepatic glycogen content at baseline after Cav3 gene transfer vs. GFP gene transfer in HepG2 cells ($n = 5$, $^*P < 0.05$). *D*: activation of IGF receptors (IGF-1R) in response to insulin ($n = 4$, NS).

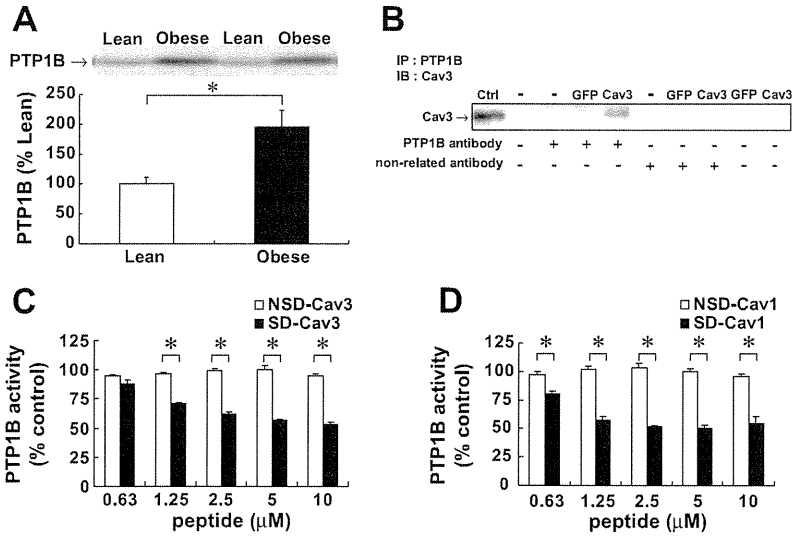

Fig. 6. Caveolin-mediated inhibition of PTP1B activity. *A*: hepatic PTP1B levels by immunoblotting in lean control and obese diabetic mice. A representative immunoblot is also shown ($n = 4$–5, $^*P < 0.05$). *B*: immunoprecipitation assays of PTP1B and Cav3 after Cav3 gene transfer vs. GFP gene transfer in diabetic obese mice. A representative immunoblot is shown. Ctrl, control. *C*: PTP1B activity was determined in the presence of increasing concentrations of scaffolding domain (SD)-Cav3 peptide or nonscaffolding domain (NSD)-Cav3 peptide ($n = 5$, $^*P < 0.05$). *D*: PTP1B activity was determined in the presence of increasing concentrations of SD-Cav1 peptide or NSD-Cav1 peptide ($n = 5$, $^*P < 0.05$).

DISCUSSION

Adenovirus-mediated gene transfer of Cav3 to the liver resulted in increased hepatic glycogen synthesis accompanied by decreased hepatic PEPCK protein levels. Insulin sensitivity, as measured by changes in FBG levels upon insulin injection and glucose tolerance test performance, were improved after Cav3 gene transfer in obese diabetic mice. A similar improvement in glucose metabolism was observed in *KKA^y* mice. Overexpression of Cav3 in cultured hepatic cells led to increased phosphorylation of IR-β and IRS in response to insulin stimulation with increased glycogen synthesis at baseline. Therefore, our findings suggest that Cav enhances insulin signals in the liver. The molecular mechanism of this enhanced insulin action may involve direct stimulation of IR by Cav, because a similar mechanism was previously proposed using purified IR and Cav peptides in vitro (30). Although we do not know the extent of caveolin-mediated inhibition of PTP1B activity in vivo, the physical interaction between PTP1B and caveolin has been reported in other studies (6). Furthermore, several investigators have demonstrated the effect of caveolin peptide administration to regulate signaling activity in cells, suggesting that such interaction of caveolin peptide occurs in living cells as well (4, 12, 25, 31).

Furthermore, as shown in the current study, direct inhibition of PTP1B by Cav may be another mechanism by which Cav enhances insulin signals. Obese diabetic mice showed an upregulation of hepatic PTP1B protein, and PTP1B activity was directly inhibited by a SD-Cav3 peptide. Increased expression of phosphatases in obesity was previously reported for other tissues (1). A physical and functional interaction between Cav and PTP1B might be responsible for the slow recovery of glucose levels in insulin tolerance tests as well as for the marked phosphorylation of IR even at low concentrations of insulin (0–1 nM) in mice with Cav3 gene transfer (Fig. 5*A*). Together, Cav3 gene transfer may be a strategy to improve glucose metabolism in vivo.

Adipose and muscle tissues are the major target organs of insulin action that abundantly express Cav1 and Cav3, respectively. Cav may play an important role in these tissues because disruption of the Cav genes, either Cav1 or Cav3, markedly impairs adipose and muscular insulin signals (7, 22). However, the role of Cav in insulin signals in the liver, another major target organ of insulin action, has been uncertain; the liver does not express abundant levels of Cav but has intact insulin signaling. Our findings have demonstrated that Cav can play an important role in insulin signals in the liver, particularly when overexpressed under pathological conditions, such as insulin resistance induced in diabetics by a high-fat diet.

Cav has been long considered a major inhibitor of growth signals and a tumor growth/proliferation suppressor (29), except in prostate cancer (18). Cav gene therapy has been proposed as a potential treatment to suppress tumor proliferation and/or metastasis in various cancers, such as breast cancer (29). Our findings suggest, however, that Cav3 plays an opposite role in insulin signaling; it stimulates IR activity, leading to enhanced IR signals.

In conclusion, Cav3 may be a conditional but important regulator of glucose metabolism. The lack of Cav impaired insulin sensitivity in adipocytes and muscles where endogenous Cav is abundantly expressed (7, 22). Although the liver does not express high levels of Cav under normal conditions, hepatic insulin signals remain intact. However, when insulin signals are impaired in diabetes, increased Cav expression in the liver improves glucose metabolism. The robust nature of our findings suggests that Cav, a membrane-anchoring protein, enhances IR signals.

ACKNOWLEDGMENTS

We thank Masahiro Sakata for technical assistance.

GRANTS

This work was supported in part by grants from the Ministry of Education, Culture, Sports, Science and Technology of Japan and by the Kitsuen Research Foundation.

DISCLOSURES

No conflicts of interest are declared by the author(s).

REFERENCES

1. **Ahmad F, Azevedo JL, Cortright R, Dohm GL, Goldstein BJ.** Alterations in skeletal muscle protein-tyrosine phosphatase activity and expression in insulin-resistant human obesity and diabetes. *J Clin Invest* 100: 449–458, 1997.
2. **Alberts P, Nilsson C, Selen G, Engblom LO, Edling NH, Norling S, Klingstrom G, Larsson C, Forsgren M, Ashkzari M, Nilsson CE, Fiedler M, Bergqvist E, Ohman B, Bjorkstrand E, Abrahmsen LB.** Selective inhibition of 11 beta-hydroxysteroid dehydrogenase type 1 improves hepatic insulin sensitivity in hyperglycemic mice strains. *Endocrinology* 144: 4755–4762, 2003.
3. **Balbis A, Baquiran G, Mounier C, Posner BI.** Effect of insulin on caveolin-enriched membrane domains in rat liver. *J Biol Chem* 279: 39348–39357, 2004.
4. **Bernatchez PN, Bauer PM, Yu J, Prendergast JS, He P, Sessa WC.** Dissecting the molecular control of endothelial NO synthase by caveolin-1 using cell-permeable peptides. *Proc Natl Acad Sci USA* 102: 761–766, 2005.
5. **Carver LA, Schnitzer JE.** Caveolae: mining little caves for new cancer targets. *Nat Rev Cancer* 3: 571–581, 2003.
6. **Caselli A, Mazzinghi B, Camici G, Manao G, Ramponi G.** Some protein tyrosine phosphatases target in part to lipid rafts and interact with caveolin-1. *Biochem Biophys Res Commun* 296: 692–697, 2002.
7. **Cohen AW, Razani B, Wang XB, Combs TP, Williams TM, Scherer PE, Lisanti MP.** Caveolin-1-deficient mice show insulin resistance and defective insulin receptor protein expression in adipose tissue. *Am J Physiol Cell Physiol* 285: C222–C235, 2003.
8. **Elchebly M, Payette P, Michaliszyn E, Cromlish W, Collins S, Loy AL, Normandin D, Cheng A, Himms-Hagen J, Chan CC, Ramachandran C, Gresser MJ, Tremblay ML, Kennedy BP.** Increased insulin sensitivity and obesity resistance in mice lacking the protein tyrosine phosphatase-1B gene. *Science* 283: 1544–1548, 1999.
9. **Galbiati F, Volonte D, Chu JB, Li M, Fine SW, Fu M, Bermudez J, Pedemonte M, Weidenheim KM, Pestell RG, Minetti C, Lisanti MP.** Transgenic overexpression of caveolin-3 in skeletal muscle fibers induces a Duchenne-like muscular dystrophy phenotype. *Proc Natl Acad Sci USA* 97: 9689–9694, 2000.
10. **Gonzalez E, Nagiel A, Lin AJ, Golan DE, Michel T.** Small interfering RNA-mediated down-regulation of caveolin-1 differentially modulates signaling pathways in endothelial cells. *J Biol Chem* 279: 40659–40669, 2004.
11. **Kawabe J, Okumura S, Lee MC, Sadoshima J, Ishikawa Y.** Translocation of caveolin regulates stretch-induced ERK activity in vascular smooth muscle cells. *Am J Physiol Heart Circ Physiol* 286: H1845–H1852, 2004.
12. **Kwiatek AM, Minshall RD, Cool DR, Skidgel RA, Malik AB, Tiruppathi C.** Caveolin-1 regulates store-operated Ca^{2+} influx by binding of its scaffolding domain to transient receptor potential channel-1 in endothelial cells. *Mol Pharmacol* 70: 1174–1183, 2006.
13. **Lampe MA, Burlingame AL, Whitney J, Williams ML, Brown BE, Roitman E, Elias PM.** Human stratum corneum lipids: characterization and regional variations. *J Lipid Res* 24: 120–130, 1983.
14. **LeRoith D, McGuinness M, Shemer J, Stannard B, Lanau F, Faria TN, Kato H, Werner H, Adamo M, Roberts CT Jr.** Insulin-like growth factors. *Biol Signals* 1: 173–181, 1992.
15. **Liu JS, Park EA, Gurney AL, Roesler WJ, Hanson RW.** Cyclic AMP induction of phosphoenolpyruvate carboxykinase (GTP) gene transcription is mediated by multiple promoter elements. *J Biol Chem* 266: 19095–19102, 1991.
16. **Maislos M, Medvedovskv V, Sztarkier I, Yaari A, Sikuler E.** *Psammomys obesus* (sand rat), a new animal model of non-alcoholic fatty liver disease. *Diabetes Res Clin Pract* 72: 1–5, 2006.
17. **Mauldin JP, Srinivasan S, Mulya A, Gebre A, Parks JS, Daugherty A, Hedrick CC.** Reduction in ABCG1 in Type 2 diabetic mice increases macrophage foam cell formation. *J Biol Chem* 281: 21216–21224, 2006.
18. **Mouraviev V, Li L, Tahir SA, Yang G, Timme TM, Goltsov A, Ren C, Satoh T, Wheeler TM, Ittmann MM, Miles BJ, Amato RJ, Kadmon D, Thompson TC.** The role of caveolin-1 in androgen insensitive prostate cancer. *J Urol* 168: 1589–1596, 2002.
19. **Oka N, Yamamoto M, Schwencke C, Kawabe J, Ebina T, Couet J, Lisanti MP, Ishikawa Y.** Caveolin interaction with protein kinase C: isoenzyme-dependant regulation of kinase activity by the caveolin scaffolding domain peptide. *J Biol Chem* 272: 33416–33421, 1997.
20. **Okumura S, Kawabe J, Yatani A, Takagi G, Lee MC, Hong C, Liu J, Takagi I, Sadoshima J, Vatner DE, Vatner SF, Ishikawa Y.** Type 5 adenylyl cyclase disruption alters not only sympathetic but also parasympathetic and calcium-mediated cardiac regulation. *Circ Res* 93: 364–371, 2003.
21. **Okumura S, Vatner DE, Kurotani R, Bai Y, Gao S, Yuan Z, Iwatsubo K, Ulucan C, Kawabe J, Ghosh K, Vatner SF, Ishikawa Y.** Disruption of type 5 adenylyl cyclase enhances desensitization of cyclic adenosine monophosphate signal and increases Akt signal with chronic catecholamine stress. *Circulation* 116: 1776–1783, 2007.
22. **Oshikawa J, Otsu K, Toya Y, Tsunematsu T, Hankins R, Kawabe J, Minamisawa S, Umemura S, Hagiwara Y, Ishikawa Y.** Insulin resistance in skeletal muscles of caveolin-3-null mice. *Proc Natl Acad Sci USA* 101: 12670–12675, 2004.
23. **Quinn PG.** Inhibition by insulin of protein kinase A-induced transcription of the phosphoenolpyruvate carboxykinase gene. Mediation by the activation domain of cAMP response element-binding protein (CREB) and factors bound to the TATA box. *J Biol Chem* 269: 14375–14378, 1994.
24. **Shiraishi S, Yamamoto R, Yanagita T, Yokoo H, Kobayashi H, Uezono Y, Wada A.** Down-regulation of cell surface insulin receptors by sarco(endo)plasmic reticulum Ca^{2+}-ATPase inhibitor in adrenal chromaffin cells. *Brain Res* 898: 152–157, 2001.
25. **Sukumaran SK, Quon MJ, Prasadarao NV.** *Escherichia coli* K1 internalization via caveolae requires caveolin-1 and protein kinase Calpha interaction in human brain microvascular endothelial cells. *J Biol Chem* 277: 50716–50724, 2002.
26. **Toya Y, Schwencke C, Couet J, Lisanti MP, Ishikawa Y.** Inhibition of adenylyl cyclase by caveolin peptides. *Endocrinology* 139: 2025–2031, 1998.
27. **Varagic VM, Mrsulja BB, Stosic N, Pasic M, Terzic M.** The glycogenolytic and hypertensive effect of physostigmine in the anti-nerve-growth-factor-serum-treated rats. *Eur J Pharmacol* 12: 194–202, 1970.
28. **Williams TM, Cheung MW, Park DS, Razani B, Cohen AW, Muller WJ, Di Vizio D, Chopra NG, Pestell RG, Lisanti MP.** Loss of caveolin-1 gene expression accelerates the development of dysplastic mammary lesions in tumor-prone transgenic mice. *Mol Biol Cell* 14: 1027–1042, 2003.
29. **Williams TM, Lisanti MP.** Caveolin-1 in oncogenic transformation, cancer, and metastasis. *Am J Physiol Cell Physiol* 288: C494–C506, 2005.
30. **Yamamoto M, Toya Y, Schwencke C, Lisanti MP, Myers MG Jr, Ishikawa Y.** Caveolin is an activator of insulin receptor signaling. *J Biol Chem* 273: 26962–26968, 1998.
31. **Zhu L, Schwegler-Berry D, Castranova V, He P.** Internalization of caveolin-1 scaffolding domain facilitated by Antennapedia homeodomain attenuates PAF-induced increase in microvessel permeability. *Am J Physiol Heart Circ Physiol* 286: H195–H201, 2004.

THE JOURNAL OF BIOLOGICAL CHEMISTRY VOL. 285, NO. 31, pp. 24248–24259, July 30, 2010

Differential Roles of Epac in Regulating Cell Death in Neuronal and Myocardial Cells*[S]

Received for publication, December 21, 2009, and in revised form, May 13, 2010 Published, JBC Papers in Press, June 1, 2010, DOI 10.1074/jbc.M109.094581

Sayaka Suzuki[‡], Utako Yokoyama[‡1], Takaya Abe[§], Hiroshi Kiyonari[§], Naoya Yamashita[¶], Yuko Kato[‡], Reiko Kurotani[‡], Motohiko Sato[‡], Satoshi Okumura[‡], and Yoshihiro Ishikawa[‡‖]

From the [‡]Cardiovascular Research Institute and [¶]Department of Molecular Pharmacology and Neurobiology, Yokohama City University Graduate School of Medicine, Yokohama 236-0004, Japan, the [§]Laboratory for Animal Resources and Genetic Engineering, RIKEN Center for Developmental Biology, Kobe 650-0047, Japan, and the [‖]Cardiovascular Research Institute, Departments of Cell Biology and Molecular Medicine, and the Department of Medicine, New Jersey Medical School-University of Medicine and Dentistry of New Jersey, Newark, New Jersey 07103

Cell survival and death play critical roles in tissues composed of post-mitotic cells. Cyclic AMP (cAMP) has been known to exert a distinct effect on cell susceptibility to apoptosis, protecting neuronal cells and deteriorating myocardial cells. These effects are primarily studied using protein kinase A activation. In this study we show the differential roles of Epac, an exchange protein activated by cAMP and a new effector molecule of cAMP signaling, in regulating apoptosis in these cell types. Both stimulation of Epac by 8-*p*-methoxyphenylthon-2′-*O*-methyl-cAMP and overexpression of Epac significantly increased DNA fragmentation and TUNEL (terminal deoxynucleotidyltransferase-mediated biotin nick end-labeling)-positive cell counts in mouse cortical neurons but not in cardiac myocytes. In contrast, stimulation of protein kinase A increased apoptosis in cardiac myocytes but not in neuronal cells. In cortical neurons the expression of the Bcl-2 interacting member protein (Bim) was increased by stimulation of Epac at the transcriptional level and was decreased in mice with genetic disruption of Epac1. Epac-induced neuronal apoptosis was attenuated by the silencing of Bim. Furthermore, Epac1 disruption *in vivo* abolished the 3-nitropropionic acid-induced neuronal apoptosis that occurs in wild-type mice. These results suggest that Epac induces neuron-specific apoptosis through increasing Bim expression. Because the disruption of Epac exerted a protective effect on neuronal apoptosis *in vivo*, the inhibition of Epac may be a consideration in designing a therapeutic strategy for the treatment of neurodegenerative diseases.

Induction of apoptosis in post-mitotic cells, such as neurons and cardiac myocytes, has been thought to be responsible for such irreversible disorders as Alzheimer and Huntington diseases as well as stroke and heart failure (1). The effect on cell death of cyclic AMP (cAMP), a major second messenger, has been extensively studied. In neuronal cells it is well known that activation of cAMP signals reduces the rate of neuronal cell death under a variety of stresses (*i.e.* β-amyloid protein, sialoglycopeptide, low potassium-induced neurotoxicity) (2–4), although there have been several reports that dopamine or prostanoid receptor-mediated cAMP production induces neurotoxicity (5, 6). β-Adrenergic receptor signaling, on the other hand, promotes apoptosis in cardiac myocytes, resulting in heart failure (7, 8). Therefore, the model proposing that cAMP signaling plays a protective role in neuronal cells but a deteriorative role in myocardial cells is well accepted.

Most studies that have demonstrated the effect of cAMP signaling on apoptosis have focused primarily on protein kinase A (PKA),[2] a classic target molecule of cAMP. Recent studies involving cAMP signaling have focused instead on Epac, an exchange protein activated by cAMP that has been identified as a new target of cAMP, independent of PKA (9). Epac has been found to regulate a variety of cellular processes, including cell proliferation, migration, secretion, and differentiation (10). It has been demonstrated that Epac either alone or with PKA plays a protective role in immune cells against apoptosis (11, 12). In post-mitotic cells such as neurons and cardiac myocytes, however, the role of Epac in apoptosis has not been reported.

To date two isoforms of Epac have been identified, Epac1 and Epac2 (9); they differ in that Epac2 contains a second binding site for cAMP. It has recently been reported that there is an up-regulation of Epac1 mRNA in Alzheimer disease (13) and an up-regulation of Epac1 protein expression in rats with inflamed neurons (14), implicating that cAMP signaling may not always play a protective role in neurons. The change in the Epac1 expression pattern has also been demonstrated in other cell

* This work was supported by a grant-in-aid for Scientific Research (KAKENHI) (to U. Y. and S. S.) and by grants from the Ministry of Health, Labor, and Welfare (to Y. I.), the Ministry of Education, Culture, Sports, Science, and Technology of Japan (to Y. I.), the Yokohama Foundation for Advanced Medical Science (to U. Y.), the Kanae Foundation for the Promotion for Medical Science (to U. Y.), the Miyata Cardiology Research Promotion Funds (to U. Y.), the Takeda Science Foundation (to U. Y.), the Sumitomo Foundation (to U. Y.), the Japan Heart Foundation Research Grant (to U. Y.), the Kowa Life Science Foundation (to U. Y.), the Cosmetology Research Foundation (to Y. I.), the Uehara Memorial Foundation (to U. Y.), the Kitsuen Research Foundation (to Y. I.), and the Japan Space Forum (to Y. I.).

[S] The on-line version of this article (available at http://www.jbc.org) contains supplemental Methods and Figs. 1–7.

[1] To whom correspondence should be addressed: Cardiovascular Research Institute, Yokohama City University Graduate School of Medicine, 3-9 Fukuura, Kanazawa-ku, Yokohama 236-0004, Japan. Tel.: 81-45-787-2575; Fax: 81-45-788-1470; E-mail: utako@yokohama-cu.ac.jp.

[2] The abbreviations used are: PKA, protein kinase A; Bim, Bcl-2 interacting member protein; pMe-cAMP, 8-*p*-methoxyphenylthon-2′-*O*-methyl-cAMP; Bnz-cAMP, N^6-benzoyladenosine-cAMP; RT, reverse transcription; TUNEL, terminal deoxynucleotidyltransferase-mediated biotin nick end-labeling; 3-NP, 3-propionic acid; siRNA, small interfering RNA; DAPI, 4′,6-diamidino-2-phenylindole; JNK, c-Jun N-terminal kinase; MAPK, mitogen-activated protein kinase; KO, knock-out.

types (*i.e.* heart, vasculature, kidney, and lung) (15–18). The stoichiometry of Epac, especially of Epac1, and that of PKA might be changed in several diseases, including neuronal and cardiac disorders; this could lead to the various effects of cAMP signaling on cell death.

Through experiments using Epac- or PKA-selective cAMP analogs and overexpression of Epac1 and the PKA catalytic subunit and Epac1-deficient mice, the present study demonstrates that cAMP signaling no longer increases neuronal cell viability when Epac is selectively activated: instead, cAMP signaling induces apoptosis through increasing Bcl-2 interacting member protein (Bim) expression. Our findings also suggest that the selective inhibition of Epac signaling may become a therapeutic strategy in the treatment of neurodegenerative diseases.

EXPERIMENTAL PROCEDURES

Antibodies and Reagents—8-*p*-Methoxyphenylthon-2′-*O*-methyl-cAMP (pMe-cAMP) and N^6-benzoyladenosine-cAMP (Bnz-cAMP) were purchased from BioLog Life Science Institute (Bremen, Germany) and Sigma, respectively. Antibodies to Epac1, Epac2, and a PKA α catalytic subunit were obtained from Santa Cruz Biotechnology (Santa Cruz, CA). An antibody to Bim was purchased from Stressgen Biotechnologies (Victoria, BC, Canada). Antibodies to Bim and cleaved caspase 3 were purchased from Cell Signaling Technology (Danvers, MA). An antibody to Bcl-2 was purchased from BD Biosciences.

Generation of Epac1 Knock-out Mice—Epac1 knock-out mice (Epac1 KO; accession number CDB0542K (LARGE (Laboratory for Animal Resources and Genetic Engineering)) were generated by means of homologous recombination (19). Briefly, the targeting vector was constructed by inserting loxP/PGK-Neo-pA/loxP (LARGE) into exon 1 and exon 2 of the genomic Epac1 locus (see Fig. 7*A*). The targeting vector was introduced into TT2 embryonic stem cells, and homologous recombinant clones were first identified by PCR, then confirmed by Southern blot analysis (see Fig. 7*B*). The targeted embryonic stem cell clones were injected into CD-1 8-cell stage embryos, and the resultant male chimeras were mated with C57BL/6 females to establish germ line transmission. All experiments were performed on C57BL/6 and CBA mixed-background 3–5-month-old male homozygous Epac1 KO and wild type (WT) littermates from F1 heterozygote crosses. Mice were genotyped by PCR using a mixture of three primers (F1, TGA GAA GAG CCC CAT CGT TGT G; B1, GCC TGG CAC ATG GAA GTG AT; NeoF1, TGA ATG GAA GGA TTG GAG CTA CG) as indicated in Fig. 7*A*. The PCR conditions consisted of 95 °C for 5 min, 35 cycles of 95 °C for 30 s each, 60 °C for 30 s, and 72 °C for 30 s followed by 72 °C for 7 min (Fig. 7*C*).

All experiments were performed on 3–5-month-old homozygous Epac1 KO mice and WT littermates. This study was approved by the Animal Care and Use Committee at Yokohama City University School of Medicine.

Primary Culture of Fetal Mouse Cortical Neurons—Primary cortical neurons were isolated from the cortices of embryonic day 15–17 C57BL/6 or Epac1 KO mice, as previously described (20) with some modifications. Briefly, the cortex was incubated with 0.3% trypsin (Invitrogen) by titration; then cells were plated onto a 12-mm glass coverslip precoated with 6 mg/ml poly-L-lysine (Wako Pure Chemical Industries, Osaka, Japan) at a density of 1×10^5 cells/glass. The cells were incubated at 37 °C with 5% CO_2, 95% atmospheric air in a neurobasal medium containing 1× GlutaMAX-1, B-27 supplement (Invitrogen), 100 μg/ml penicillin, and 100 μg/ml streptomycin. Cells were used in experiments 4–7 days later.

Primary Culture of Neonatal Mouse Cardiac Myocytes—Cardiac myocytes were isolated from the hearts of 1-day-old mice as previously described (21) with some modifications. Briefly, myocytes were chopped into small pieces and digested with 0.1% collagenase type II and 0.04% pancreatin 3 times at 7-min intervals. To remove the non-myocyte fraction, the cells were plated onto culture dishes in minimum essential medium (Invitrogen) with 10% fetal bovine serum containing 100 μg/ml penicillin and 100 μg/ml streptomycin for 45 min, after which the non-attached myocyte-rich fraction was plated onto a 12-mm glass coverslip precoated with 20 mg/ml laminin (Sigma) at a density of 1×10^5 cells/glass in the same medium. Twenty-four hours after plating, the culture medium was changed to minimum essential medium with an insulin-transferrin-selenium-A supplement (ITS-A, Invitrogen) containing 100 μg/ml penicillin and 100 μg/ml streptomycin. The cells were maintained in a humidified 5% CO_2, 95% atmospheric air incubator at 37 °C.

Primary Culture of Mouse Renal Epithelial Cells—Primary culture of mouse renal epithelial cells was performed as previously described (22).

Quantitative Reverse Transcription (RT)-PCR—Total RNA was extracted from cortical neurons using TRIzol (Invitrogen) according to the manufacturer's instructions. Both the generation of cDNA and the RT-PCR analysis were performed as previously described (17, 23). Real-time PCR was executed using a MyiQ Single-Color Real-Time PCR Detection System (Bio-Rad) and an SYBR Green kit (Takara Bio, Shiga, Japan). Primers for amplification were designed based on Bim (5′-CCCGGAGATACGGATTGCAC-3′ and 5′- GCCTCGCGGTAATCATTTGC-3′) and 18 S ribosomal RNA. The forward and reverse primer set was designed between multiple exons. Abundance of mRNA was determined relative to that of 18 S ribosomal RNA.

Northern Blotting—Partial fragments of mouse Epac1 and Epac2 cDNA clones were obtained by PCR. A mouse glyceraldehyde-3-phosphate dehydrogenase probe was used as an internal control. Northern blotting was performed as previously described (24).

Western Blot Analysis—Western blot analysis of cortical neurons and cardiac myocytes was performed as previously described (25) with some modifications. Briefly, cells in 35-mm plastic dishes were lysed and collected with a lysis buffer (25 mM Tris-HCl (pH 8.0), 10 mM EGTA, 10 mM EDTA, 10 mM $Na_4P_2O_7$, 100 mM NaF, 10 mM Na_3VO_4, 20 μg/ml 1-chloro-3-tosylamido-7-amino-2-heptanone or N^{α}-*p*-tosyl-L-lysine chloromethyl ketone, 10 μg/ml leupeptin, 1 mM phenylmethylsulfonyl fluoride, 50 units of erythrina trypsin inhibitor, 2 μg/ml aprotinin, and 1% Nonidet P-40). After protein concentrations were determined using the RC DC protein assay kit (Bio-Rad), SDS-PAGE and Western blotting were performed followed by densitometric analysis using LAS3000 and Science Lab Multi Gauge Version 3.0 software (Fujifilm, Tokyo, Japan).

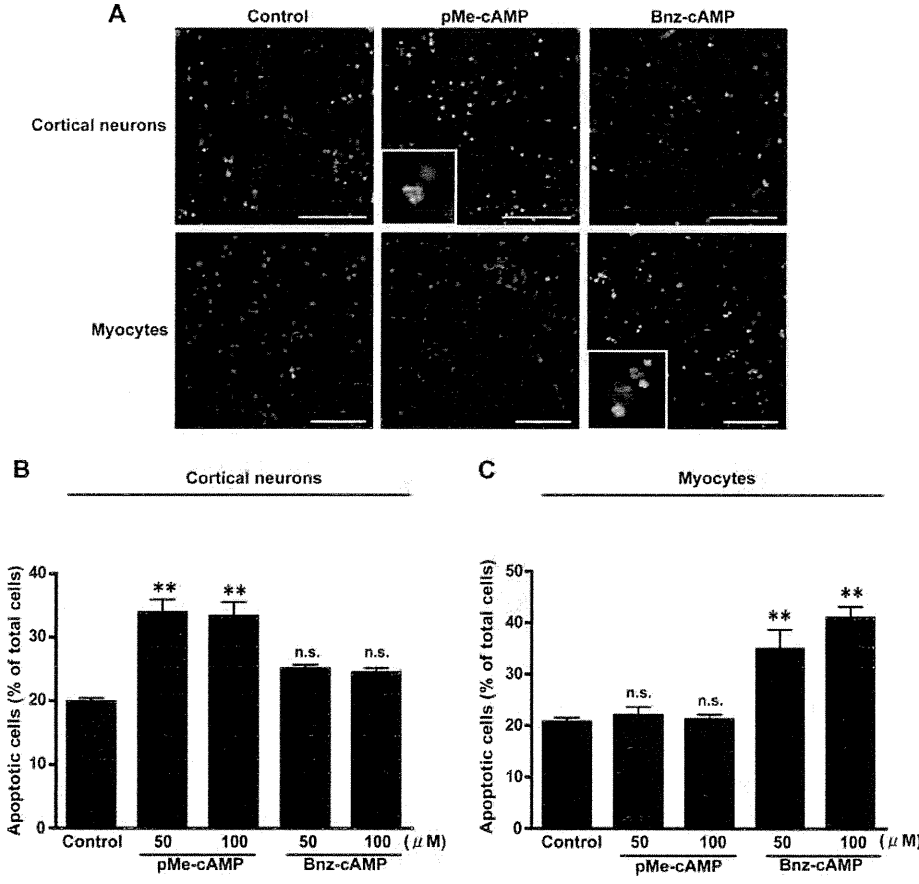

FIGURE 1. **Effects of activation of Epac and PKA on apoptosis in cortical neurons and cardiac myocytes.** *A*, apoptotic cells (*green*) in cortical neurons and myocytes were examined by means of TUNEL staining 48 h after treatment with pMe-cAMP (50 μM) or Bnz-cAMP (50 μM). Nuclei were stained with DAPI (*blue*). *Scale bar*, 100 μm. The *inset* is magnified five additional times. *B* and *C*, quantification of TUNEL-positive cells by counting nuclei in cortical neurons and cardiac myocytes is shown. The results are presented as percentages of the total cell number. $n = 6$ from 3 independent experiments. **, $p < 0.01$ *versus* control. *n.s.*, not significant.

Immunoprecipitation—Lysates from cells treated with pMe-cAMP or Bnz-cAMP for 24 h were incubated with 2 μg of anti-Bcl-2 or anti-Bim antibody overnight. Immune complexes were captured with protein G-Sepharose 4 Fast Flow (GE Healthcare). Beads were washed 3 times in the lysis buffer and boiled in an SDS sample buffer. Samples were subjected to SDS-PAGE and blotted onto a polyvinylidene difluoride membrane (Immobilon-P; Millipore, Billerica, MA).

Adenovirus Construction—For construction of adenoviral vectors, full-length cDNA-encoding human Epac1, Epac2, and PKA α catalytic subunits were cloned into an adenoviral vector using an AdenoX adenovirus construction kit (Clontech, Mountain View, CA) (17). Human Epac1 and Epac2 cDNAs were kindly provided by Dr. J. L. Bos of University Medical Center, Utrecht, The Netherlands. Adenovirus-mediated transfection was performed using LacZ control. The cells were infected with adenoviruses at the indicated multiplicities of infection and used for their corresponding assays 24 h later.

Transfection of siRNA in Cortical Neurons—Silencing of Bim was carried out using Accell SMARTpool siRNAs (Dharmacon Inc., Lafayette, CO), each of which contains four siRNAs designed for use with the Bim gene (5′-CUGGCUUCCUUUACGUUUU-3′, 5′-CUAUGAAUUGUAGAAGUAU-3′, 5′-CGCUUAUUUAA-AUGUCUUA-3′, and 5′-UCAUAA-UUAAGGAUUUGUA-3′) according to the manufacturer's instructions. Briefly, 48 h after plating, cortical neurons were transfected with 1 μM siRNA and subsequently cultured in a neurobasal medium. The efficiency of the knockdown of the Bim protein was evaluated 72 h after transfection by Western blot analysis. Scrambled siRNAs for Bim-targeted siRNA (Dharmacon Inc.) were used as a negative control.

Terminal Deoxynucleotidyltransferase-mediated Biotin Nick End-labeling (TUNEL) Assay—*In situ* labeling of fragmented DNA in cultured cortical neurons and cardiac myocytes was performed using the DeadEnd™ fluorometric TUNEL system (Promega, Madison, WI) according to the manufacturer's instructions. Cells were incubated with the presence or absence of pMe-cAMP or Bnz-cAMP for 48 h, fixed with 4% paraformaldehyde for 25 min, and then incubated with 0.2% Triton X-100 for 5 min. The cells were equilibrated with a buffer consisting of 200 mM potassium cacodylate (pH 6.6), 25 mM Tris-HCl (pH 8.0), 0.2 mM dithiothreitol, 0.25 mg/ml bovine serum albumin, and 2.5 mM cobalt chloride at room temperature for 10 min followed by 60 min of incubation with a terminal deoxynucleotidyltransferase reaction buffer containing 100 μM dATP, 5 μM fluorescein-12-dUTP, 10 mM Tris-HCl (pH 7.6), 1 mM EDTA, and 40 μM terminal deoxynucleotidyltransferase enzyme at 37 °C. DNAs were stained with DAPI (4′, 6-diamidino-2 phenylindole). The percentage of the total cells that were TUNEL-positive was determined in a blinded manner. Approximately 2000–3000 cells in 10 randomly selected fields from each sample were counted. For detection of apoptosis in brain tissues from WT or Epac1 KO mice, deparaffinized tissue sections were treated with 20 μg/ml proteinase K and 50 mM EDTA in 100 mM Tris-HCl (pH 8.0). The sections were fixed with 4% paraformaldehyde for 15 min at room temperature and then subjected to the equilibration step in the procedures described above.

Analysis of DNA Fragmentation by Enzyme-linked Immunosorbent Assay—Histone-associated DNA fragments were quantified using the Cell Death Detection enzyme-linked immunosorbent assay kit (Roche Diagnostics) according to the manufacturer's instructions. After cortical neurons and cardiac myocytes were incubated in the presence or absence of pMe-cAMP or Bnz-cAMP for 48 h, they were gently washed with phosphate-buffered saline and incubated with a lysis buffer

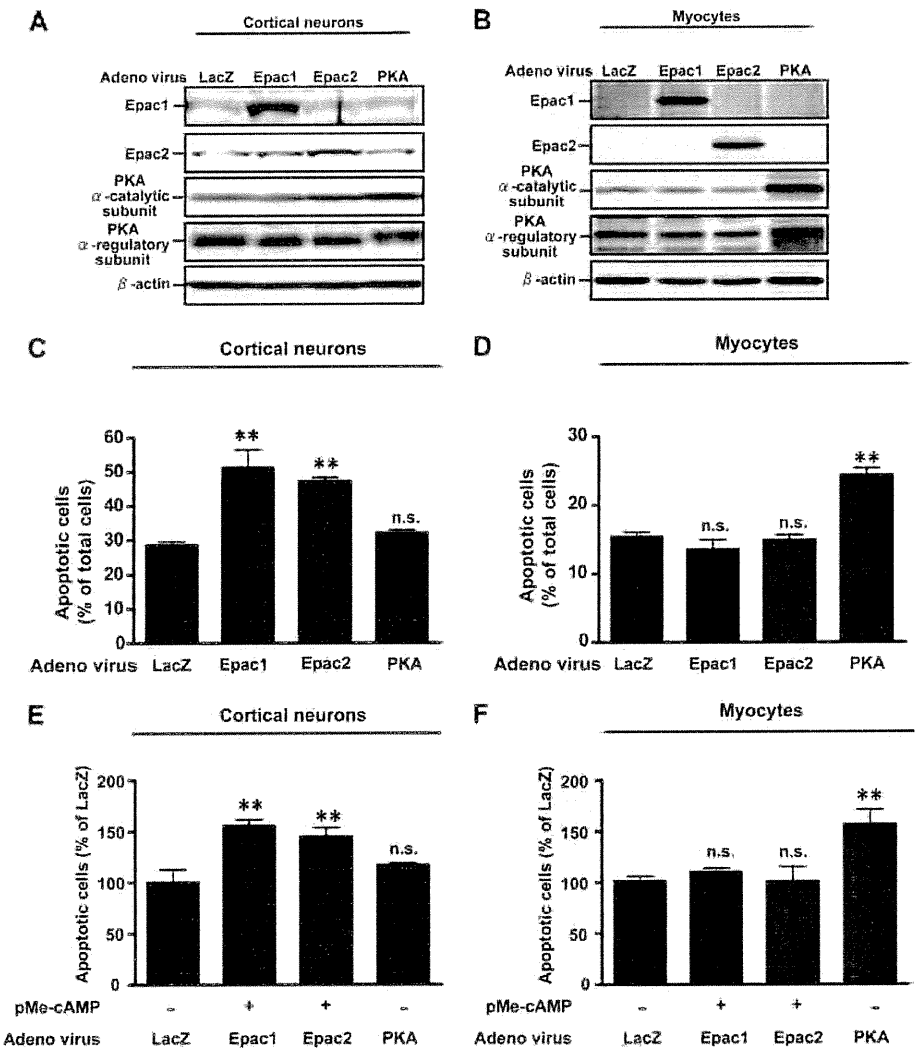

FIGURE 2. **Effects of overexpression of Epac and PKA on apoptosis in cortical neurons and cardiac myocytes.** *A*, shown are the representative immunoblots of cortical neurons or myocytes transfected with Epac1, Epac2, PKA α catalytic subunit, PKA regulatory subunit, and LacZ for 12 h (multiplicity of infection = 2). β-Actin served as an internal control. *C–F*, apoptosis was evaluated by means of TUNEL staining (*C* and *D*) and cell death detection enzyme-linked immunosorbent assay (*E* and *F*) 48 h after incubation with indicated adenovirus and an Epac-selective cAMP analog in cortical neurons and cardiac myocytes. The results are presented as percentages of the total cell number. $n = 4-8$ from 2 independent experiments. **, $p < 0.01$, *versus* LacZ control. *n.s.*, not significant.

(phosphate-buffered saline containing 10 mM EDTA (pH 7.2) and 0.1% Triton-X) for 1 h at 37 °C followed by vigorous shaking for 30 s. The cell lysates containing cytoplasmic histone-associated DNA fragments were applied to a streptavidin-coated microtiter plate. Subsequently, a mixture of biotin-labeled anti-histone antibody and peroxidase-conjugated anti-DNA antibody was added, and the resulting mixture was incubated with moderate shaking for 2 h. After unbound antibodies were removed by washing, the amount of nucleosomes was quantified based on the peroxidase retained in the immune complex. The activity of the peroxidase was determined photometrically using 2,2-azino-di-[3-ethylbenzthiazoline-sulfonate] as a substrate. The values from triplicate absorbance (at 405 nm) measurements were then averaged.

Mitochondrial Membrane Potential Analysis—Mitochondrial membrane potential of cortical neurons was quantified using a Mitocapture™ Mitochondrial Apoptosis Detection kit (BioVision Inc., Mountain View, CA) according to the manufacturer's instructions. Cortical neurons were incubated on a 12-mm glass coverslip in the presence or absence of pMe-cAMP or Bnz-cAMP for 48 h, then stained with Mitocapture reagent and incubated in DAPI to allow the visualization of all nuclei. The images were obtained using an inverted microscope (TE2000-E, Nikon, Japan). The red emission of the dye detected at 543 nm is due to a potential-dependent aggregation in the mitochondria reflecting normal membrane potential. Green fluorescence detected at 488 nm reflects the monomeric form of Mitocapture™, appearing in the cytosol after mitochondrial membrane depolarization. The percentage of the total cells representing apoptotic cells was determined in a blinded manner by counting ~1000–3000 cells in 10 randomly selected fields from each sample.

Rap1 Activation Assay—Rap1 activity was measured using the EZ-Detect RAP1 activation kit (Pierce) according to the manufacturer's instructions. Primary renal epithelial cells from WT and Epac1 KO mice were lysed 15 min after stimulation with pMe-cAMP (50 μM). Cell lysates were incubated with the Rap binding domain RalGDS-RBD fused to a glutathione *S*-transferase disk. After cells were washed several times, bound GTP-Rap1 was removed from the disk through boiling in an SDS sample buffer and analyzed by Western blotting using an anti-Rap1 antibody.

In Vivo Experiment and Tissue Preparation—3-Propionic acid (3-NP, Sigma) was prepared and administered as previously described (26). 3-NP was dissolved in saline, and the resulting solution was adjusted to pH 7.3–7.4 with 5 N NaOH. 3-NP (140 mg/kg/day) was the injected intraperitoneally into the animals once per day for 2 days. Twenty-four hours after the second injection, the mice were anesthetized with pentobarbital and transcardially injected with 10% paraformaldehyde/phosphate-buffered saline (pH 7.4). Brains were fixed in the same fixative solution overnight, immersed in 70% ethanol for 24 h, then embedded in paraffin. Sections 4 μm in thickness were subjected to TUNEL staining.

Statistical Analysis—All data are reported as the mean ± S.E. Comparisons between two groups were analyzed using Student's *t* test. For multiple groups, one-way analysis of variance

was used with a Bonferroni post-hoc test. $p < 0.05$ was considered to indicate significance.

RESULTS

Differential Effects of Epac on Apoptosis in Mouse Cortical Neurons and Myocytes—We first investigated whether the stimulation of Epac has similar effects on apoptosis in various kinds of post-mitotic cells using a primary culture of mouse cortical neurons and cardiac myocytes. Apoptosis was detected by means of TUNEL staining 48 h after treatment with pMe-cAMP or Bnz-cAMP, the Epac- and PKA-selective cAMP analogs, respectively (27). We observed strong TUNEL labeling of apoptotic bodies in cortical neurons treated with pMe-cAMP (Fig. 1*A*, *upper panels*, *inset*). In contrast, pMe-cAMP did not induce apoptosis in cardiac myocytes (Fig. 1*A*, *lower panels*). The number of TUNEL-positive cells was quantified, showing that stimulation of Epac significantly increased apoptosis in cortical neurons but not in cardiac myocytes (Fig. 1, *B* and *C*). Because a high Bax/Bcl-2 ratio is associated with greater vulnerability to apoptotic activation (28, 29), we quantified the protein expression of Bax/Bcl-2 to confirm our findings. Activation of Epac by pMe-cAMP increased the Bax/Bcl-2 ratio in cortical neurons but not in cardiac myocytes (supplemental Fig. 1, *A–D*).

It is already known that activation of cAMP/PKA signaling plays a protective role in neuronal cells but a deteriorative role in myocardial cells (30, 31). In accordance with previous reports, the PKA-selective cAMP analog Bnz-cAMP induced apoptosis in cardiac myocytes but not in cortical neurons, even at 100 μM (Fig. 1, *A–C*). These results suggest that the activation of Epac has different effects on apoptosis in neuronal cells and cardiac myocytes.

Effects of Overexpression of Epac on Apoptosis in Cortical Neurons and Cardiac Myocytes—To confirm that Epac was involved in neuronal cell death, we performed adenovirus-mediated gene transfer of Epac1 and Epac2 (as both isoforms of Epac (9) are known to be activated by pMe-cAMP), a PKA α catalytic subunit, or a LacZ control. Overexpression of Epac1, Epac2, PKA α catalytic subunit proteins, or PKA α regulatory subunit proteins in cortical neurons and cardiac myocytes 12 h after infection with each adenovirus is shown in Fig. 2, *A* and *B*. Endogenous protein expression of Epac1, Epac2, and PKA subunits was not significantly affected by any of the adenoviruses. We also confirmed that overexpression of PKA α catalytic subunit significantly increased PKA activity in cortical neurons (supplemental Fig. 2). Overexpression of Epac1 or Epac2, unlike LacZ, significantly increased the incidence of TUNEL-positive apoptotic cells in cortical neurons but not in cardiac myocytes (Fig. 2, *C* and *D*). In contrast, overexpression of PKA increased the number of TUNEL-positive cells in cardiac myocytes but not in cortical neurons. An enzyme-linked immunosorbent assay yielded results similar to those of TUNEL staining (Fig. 2, *E* and *F*), indicating that overexpression of Epac1 or Epac2 increased DNA fragmentation in cortical neurons but not in cardiac myocytes. Importantly, these results are different from those obtained through PKA overexpression, suggesting that, at least in part, Epac promotes neuronal, but not myocardial, apoptosis.

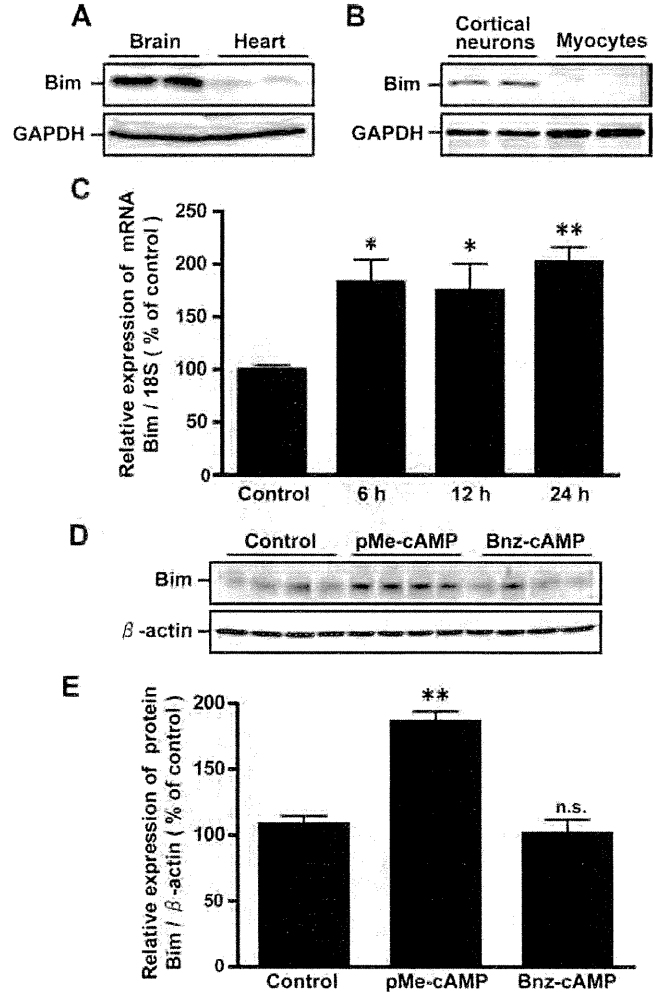

FIGURE 3. **Activation of Epac increased the expression of Bim mRNA and protein in cortical neurons.** *A* and *B*, shown is expression of endogenous Bim protein in brain and heart tissues (*A*) and cultured cortical cells and cardiac myocytes (*B*). *C*, the expression of Bim mRNA in cortical neurons was quantified using real-time RT-PCR. The data are normalized to 18 S ribosomal RNA. *D*, shown are representative immunoblots of Bim 24 h after the addition of pMe-cAMP (50 μM) or Bnz-cAMP (50 μM) in cortical neurons. β-Actin served as an internal control. *E*, shown is quantification of cAMP analog-induced Bim expression from three independent experiments. The results are presented as percentages of the amount of Bim expressed in the control experiment. $n = 6–8$, **, $p < 0.01$ *versus* control. *GAPDH*, glyceraldehyde-3-phosphate dehydrogenase.

Epac Activation Increases Bim Expression—The Bcl-2 interacting member (Bim) is a sensor of apoptotic stress located upstream of the Bcl-2 family. Bim regulates Bcl-2 in the mitochondrial membrane, resulting in apoptosis (32, 33). Bim protein was highly expressed in brain tissue and cortical neurons (Fig. 3, *A* and *B*) but was expressed either slightly or not at all in heart tissue and cardiac myocytes, as previously described (34, 35). A previous paper suggested the involvement of cAMP/PKA signaling in regulating Bim expression in lymphoid cells (55). We, therefore, examined the change in the expression levels of Bim mRNA and protein in cortical neurons using pMe-cAMP. We found that pMe-cAMP increased expression of Bim mRNA and protein in a time-dependent manner (Fig. 3*C* and see Fig. 5, *C* and *F*). Furthermore, pMe-cAMP, but not Bnz-cAMP, signif-

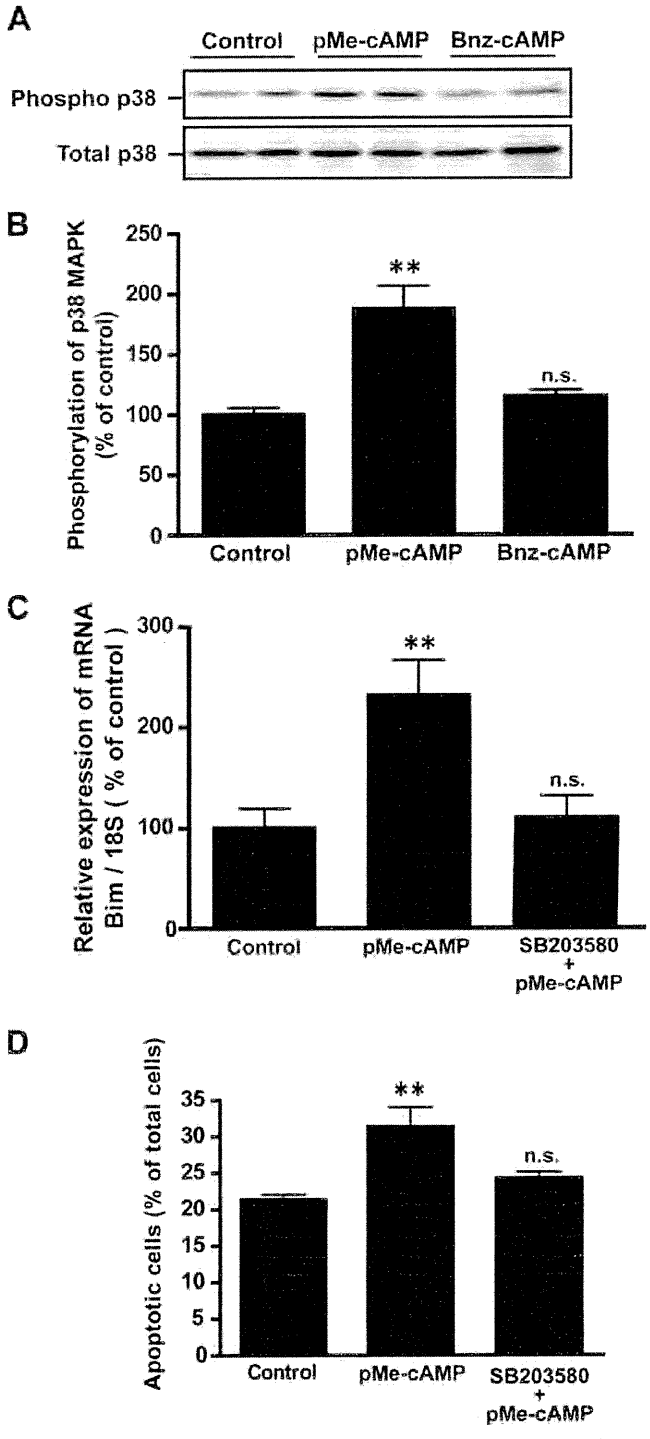

FIGURE 4. **Effect of p38 MAPK on Epac-induced Bim expression and apoptosis in cortical neurons.** *A* and *B*, shown are representative images and quantification of phosphorylation/total p38 protein in mouse cortical neurons treated with pMe-cAMP (50 μM) or Bnz-cAMP (50 μM) for 24 h. The results are presented as percentages of the amount of phosphorylation observed in the control experiment. $n = 6$ from 3 independent experiments. **, $p < 0.01$ *versus* control. *C*, the expression of Bim mRNA 24 h after the addition of pMe-cAMP (50 μM) or SB203580 (10 μM) plus pMe-cAMP (50 μM) in cortical neurons was quantified using real-time RT-PCR. The data are normalized to 18 S ribosomal RNA. $n = 6-8$; **, $p < 0.01$ *versus* control. *D*, apoptotic cells in cortical neurons and myocytes were examined by means of TUNEL staining 48 h after treatment with pMe-cAMP (50 μM) or SB203580 (10 μM) plus pMe-cAMP (50 μM). TUNEL-positive cells were quantified by counting nuclei in cortical neurons. The results are presented as percentages of the total cell number. $n = 4-6$; **, $p < 0.01$ *versus* control. *n.s.*, not significant.

icantly increased Bim protein in cortical neurons 24 h after treatment (Fig. 3,*D* and *E*). These results suggest that the stimulation of Epac increases Bim expression by enhancing transcription in cortical neurons, although the stimulation of PKA does not.

Inhibition of p38 MAPK Attenuates Epac-induced Bim Expression and Apoptosis—Three signal pathways have been implicated in regulating Bim protein expression: the JNK/c-Jun, cell cycle (Cdk4/E2F/Myb), and p38MAPK/FoxO pathways (36, 37). We next sought to determine which of these pathways plays the most important role. We found that an Epac-selective cAMP analog increased phosphorylation of p38 MAPK in cortical neurons, although a PKA-selective cAMP analog did not (Fig. 4, *A* and *B*). In contrast, there was no significant difference between Epac and PKA stimulation in terms of their effects on the phosphorylation of p44/42 MAPK, JNK1, or JNK2/3 (data not shown). Furthermore, SB203580, a p38 MAPK inhibitor, attenuated Epac-induced Bim expression and apoptosis (Fig. 4, *C* and *D*). These results suggest that Epac-induced neuronal apoptosis is mediated by the elevation of Bim expression via p38 MAPK.

Epac Activation Increases Interaction of Bim with Bcl-2—Bim is thought to exert its pro-apoptotic activity by binding to Bcl-2, thereby blocking the anti-apoptotic function of Bcl-2 (38). After demonstrating that stimulation of Epac increased Bim expression, we needed to confirm that the binding of Bim to Bcl-2 was likewise increased. We conducted pulldown assays using anti-Bcl-2 and anti-Bim antibodies after treatment with pMe-cAMP or Bnz-cAMP and found that the activation of Epac by pMe-cAMP significantly increased the amount of Bim associated with Bcl-2 in cortical neurons 24 h after the treatment (Fig. 5, *A* and *D*). Association of Bim with Bcl2 was also increased 10 h after Epac activation (Fig. 5, *B* and *E*), suggesting that association of Bim with Bcl2 was increased in accordance with increased Bim expression. Activation of PKA by Bnz-cAMP did not promote binding Bcl-2 with Bim even 24 h after treatment (Fig. 5, *H* and *I*).

Because it is already known that Bcl-2 regulates the mitochondrial pathway of apoptosis, we next explored whether pMe-cAMP induced apoptosis through the mitochondrial pathway in cortical neurons. Disruption of mitochondrial transmembrane potential is one of the earliest intracellular events, and such disruption occurs after induction of apoptosis via mitochondria (1). In apoptotic cells, the mitochondrial membrane potential is dissipated, and thus, the Mitocapture dye is dispersed in the cell as green fluorescent monomers detected at 488 nm. We found that Epac activation with pMe-cAMP (50 μM) promoted the disruption of mitochondrial transmembrane potential based on 488-nm-positive (green fluorescence) intensity in cortical neurons (Fig. 5, *J* and *K*). Taken together, these data suggest that stimulation of Epac promotes the binding of Bim to Bcl-2, leading to neuronal apoptosis via the mitochondrial pathway.

Epac-induced Neuronal Apoptosis Is Mediated by Bim—To further confirm the contribution of Bim to Epac-induced apo-

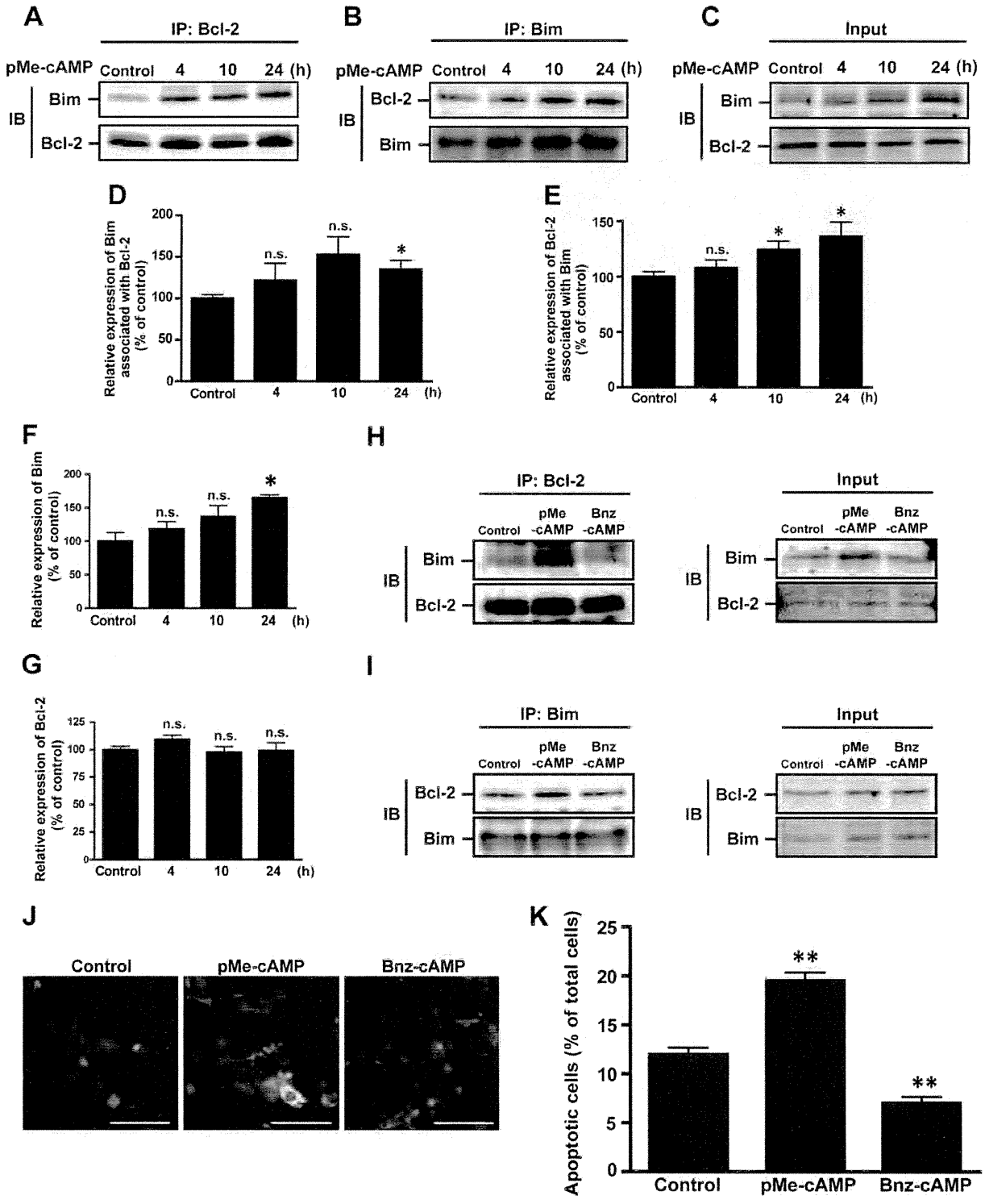

FIGURE 5. **Activation of Epac promoted interaction between Bcl-2 and Bim protein and decreased mitochondrial transmembrane potential in cortical neurons.** *A–C*, a representative immunoblot (*IB*) shows the interaction between Bcl-2 and Bim protein was increased by treatment with pMe-cAMP (50 μM) in a time-dependent manner. *IP*, immunoprecipitate. *D–G*, the pixel intensity of the bands obtained in each experiment was calculated. The results are presented as percentages of the intensity of the corresponding bands in the control experiment. $n = 5$ from 5 independent experiments. *n.s.*, not significant. **, $p < 0.05$ *versus* control. *H* and *I*, interaction of Bim and Bcl-2 in cortical neurons 24 h after incubation with pMe-cAMP (50 μM) or Bnz-cAMP (50 μM) was observed by means of immunoprecipitation with an antibody to Bim or Bcl-2. *J*, the changes in mitochondrial transmembrane potential were detected using the MitoCapture Apoptosis detection kit 48 h after the addition of pMe-cAMP (50 μM) or Bnz-cAMP (50 μM) in cortical neurons. Representative photomicrographs of cortical neurons stained with a cationic dye that fluoresces red in intact cells and green in apoptotic cells are shown. All nuclei were stained with DAPI (*blue*). *Scale bar*, 50 μm. *K*, apoptotic cells were counted, and their incidence was calculated. The results are presented as percentages of the total cell number. $n = 4$; **, $p < 0.01$ *versus* control.

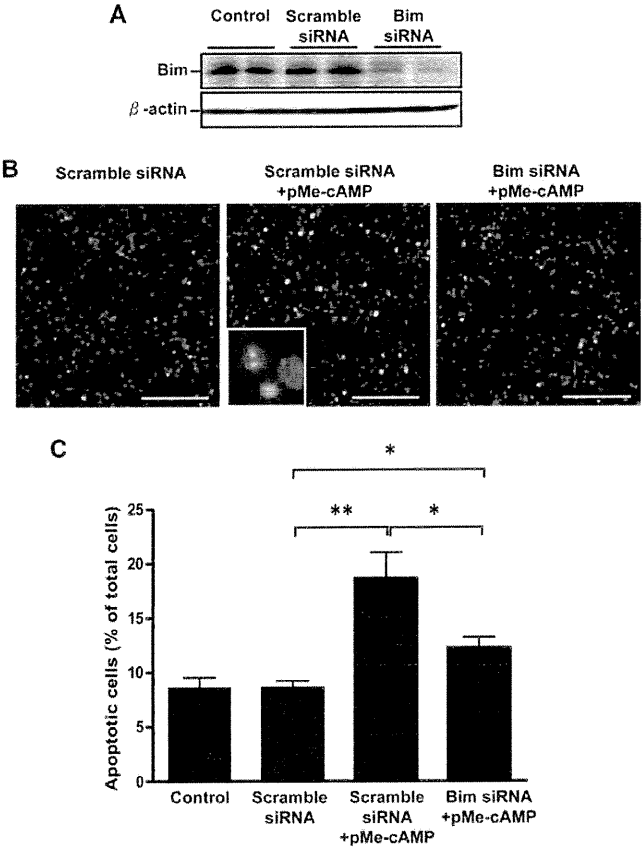

FIGURE 6. **Silencing of Bim attenuated Epac-induced apoptosis in cortical neurons.** *A*, shown is a representative immunoblot of Bim 72 h after transfection of Bim-targeted siRNA or negative siRNA control in cortical neurons. *B*, cortical neurons were transfected with indicated siRNA for 72 h, then treated with pMe-cAMP (50 μM) for 48 h. Apoptotic cells (*green*) were analyzed for TUNEL staining. All nuclei were stained with DAPI (*blue*). *Scale bar*, 100 μm. *C*, TUNEL-positive cells were quantified by counting nuclei in cortical neurons. The results are presented as percentages of the total cell number. $n = 4$; **, $p < 0.01$; *, $p < 0.05$ *versus* scramble siRNA. *n.s.*, not significant.

ptosis is in cortical neurons, we used Bim-targeted siRNA. Changes in Bim protein expression caused by the siRNAs are shown in Fig. 6*A*. When Bim was silenced, the effect of pMe-cAMP on the number of TUNEL-positive cells in cortical neurons became significantly smaller (Fig. 6, *B* and *C*), although Epac-induced apoptosis was not completely abolished. The evidence suggests that enhanced Bim expression via p38 MAPK appears to play an important role in Epac-induced apoptosis in neuronal cells.

Effects of Apoptotic Stimuli on Cortical Neurons of Epac1 KO Mice—Two isoforms of Epac, Epac1 and Epac2, have been previously identified (9) and are known to be activated by pMe-cAMP. In the present study we focused on the role of Epac1, because changes in Epac1 expression have been demonstrated in Alzheimer disease and in neuronal cells (13–15). It has, therefore, been tentatively proposed that Epac inactivation might play a protective role against neuronal apoptosis.

To test this theory, we generated Epac1 KO mice (see "Experimental Procedures" and Fig. 7*A*), which lacked Epac1 expression in neuronal cells as shown by Northern blot analysis (Fig. 7*D*). pMe-cAMP-induced Rap1 activation in Epac1 KO mice was significantly decreased in renal epithelial cells (Fig. 7*E*). Because renal epithelial cells do not express Epac2, this decrease in Rap1 activation most likely mirrors the impact of Epac1 deletion.

Induction of neuronal apoptosis has been well demonstrated in cortical neuronal cells using 3-NP (26, 39) or hydroxyl peroxide (40, 41). Using these pharmacological stressors, we examined whether the induction of apoptosis could be altered in cultured neuronal cells obtained from Epac1 KO mice. Apoptosis induced by hydroxyl peroxide or 3-NP, an irreversible inhibitor of mitochondria complex II, and detected through TUNEL staining was significantly decreased in neuronal cells from Epac1 KO mice (Fig. 8, *A* and *B*). Furthermore, both mRNA and protein expression levels of Bim remained significantly lower in cells from Epac1 KO mice than in those from WT mice (Fig. 8, *C–E*), suggesting that Epac1 deletion plays a protective role against neuronal stresses.

Deletion of Epac1 Attenuates 3-NP-induced Neuronal Apoptosis in Vivo—To examine the effect of Epac1 deletion *in vivo*, we administered 3-NP systemically to intact mice; this is a chemical and pathological way to induce mitochondrial and degenerative disorders *in vivo* (26, 39). We determined the number of apoptotic cells in cortical and striatal regions of Epac1 KO and WT mice through TUNEL staining. We found that 3-NP-induced apoptosis was significantly decreased in both the cortices and the striata of Epac1 KO mice *in vivo* (Fig. 9, *A*, *B*, *D*, and *E*). We confirmed that TUNEL-positive cells were stained with NeuN, a neuron-specific marker (supplemental Fig. 3). Furthermore, the number of cleaved caspase 3-positive cells was significantly increased in WT mice treated with 3-NP and was attenuated in Epac1 KO mice treated with 3-NP (Fig. 9, *A*, *C*, *D*, and *F*).

Taken together, these results reveal that Epac plays an important role in inducing neuronal, but not myocardial, apoptosis. More importantly, its role in this process is different from that of PKA. We found that neuronal apoptosis was, at least partially, mediated by Epac-Bim signaling and that Epac silencing had a protective role against apoptosis *in vivo*. Inhibition of Epac might be considered as a therapeutic strategy for the treatment of neurodegenerative diseases.

DISCUSSION

It is well known that cAMP signaling increases neuronal cell survival and decreases myocardial cell survival. We have demonstrated here that the activation of cAMP signaling does not protect neuronal cells when Epac is selectively activated. Rather, cAMP signaling increased apoptosis in neuronal cells when Epac1 was activated. In myocardial cells, however, Epac activation does not promote apoptosis. To our knowledge this is the first demonstration of the differential role of Epac in apoptosis in neuronal and myocardial cells, both of which are typical post-mitotic cells. The present study suggests that neuronal apoptosis is partly mediated by Epac through increased Bim expression and that the inhibition of Epac signaling plays a protective role in neuronal apoptosis *in vivo*.

The Roles of Epac and PKA in Apoptosis—The effect of cAMP signaling on cell death has been explored in multiple cell types, although most of these studies were conducted before Epac was

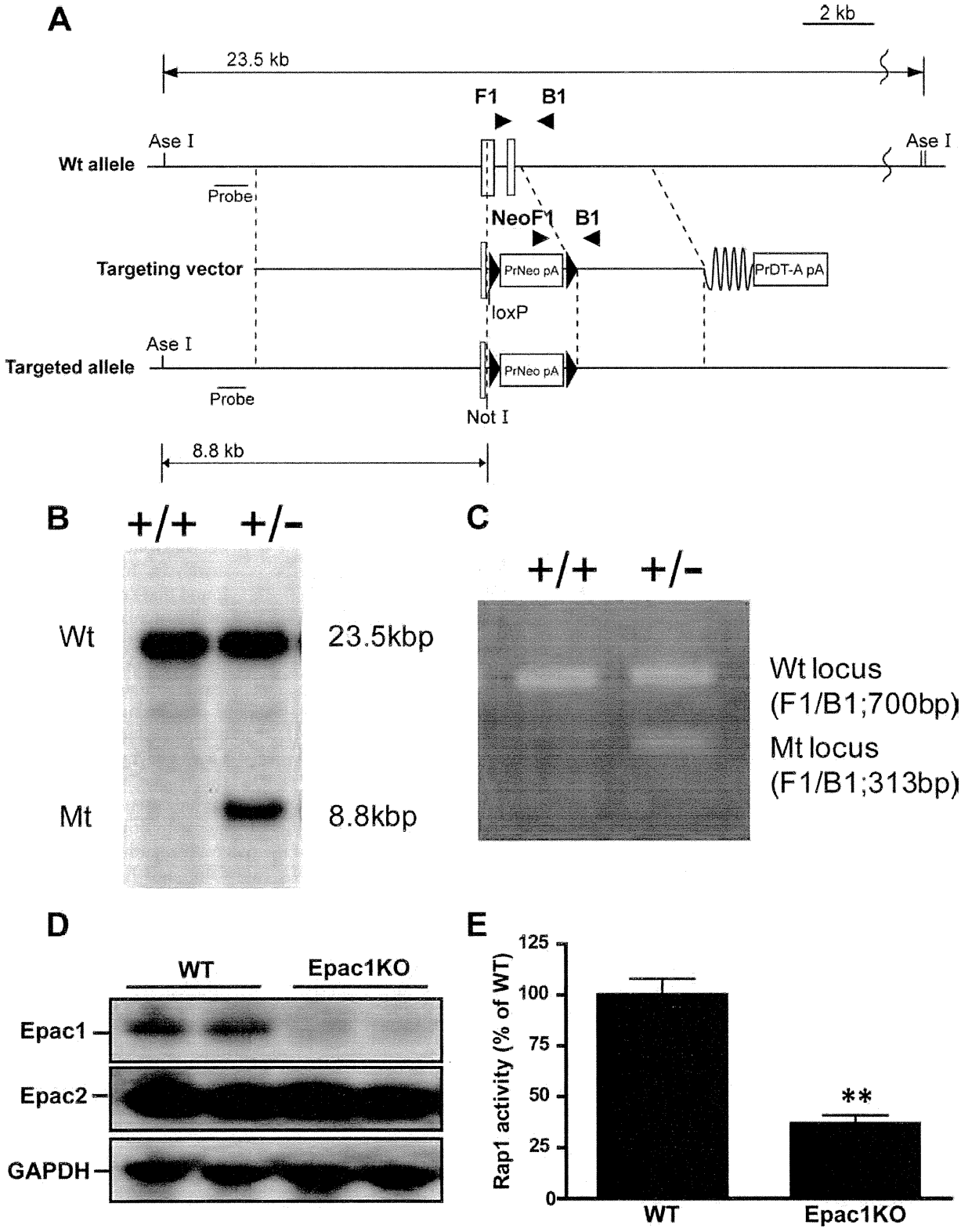

FIGURE 7. **Generation of Epac1 gene-targeted mice.** *A*, targeted disruption of the Epac1 gene is shown. The partial structure of the Epac1 gene (WT) and the resultant mutated allele (Epac1 KO) are shown. The positions of the phosphoglycerate kinase promoter neo cassette (*Neo*) and 5′-probe are indicated. *B*, shown is a Southern blot analysis of targeted embryonic stem cell (*ES*) clones. Genomic DNA from control TT2 ES cells and homologous targeted clones was digested with AseI and Not1 and hybridized with the probe as indicated in *A*. *C*, genotyping mice by PCR is shown. *D*, Northern blot analysis of Epac1, Epac2, and glyceraldehyde-3-phosphate dehydrogenase (*GAPDH*) in the brains of WT and Epac1 KO mice is shown. *E*, Rap1 activation of renal epithelial cells from WT and Epac1 KO mice 15 min after treatment with pMe-cAMP (50 μM) is shown. The data are normalized to total Rap1. $n = 4$; **, $p < 0.01$ *versus* WT mice.

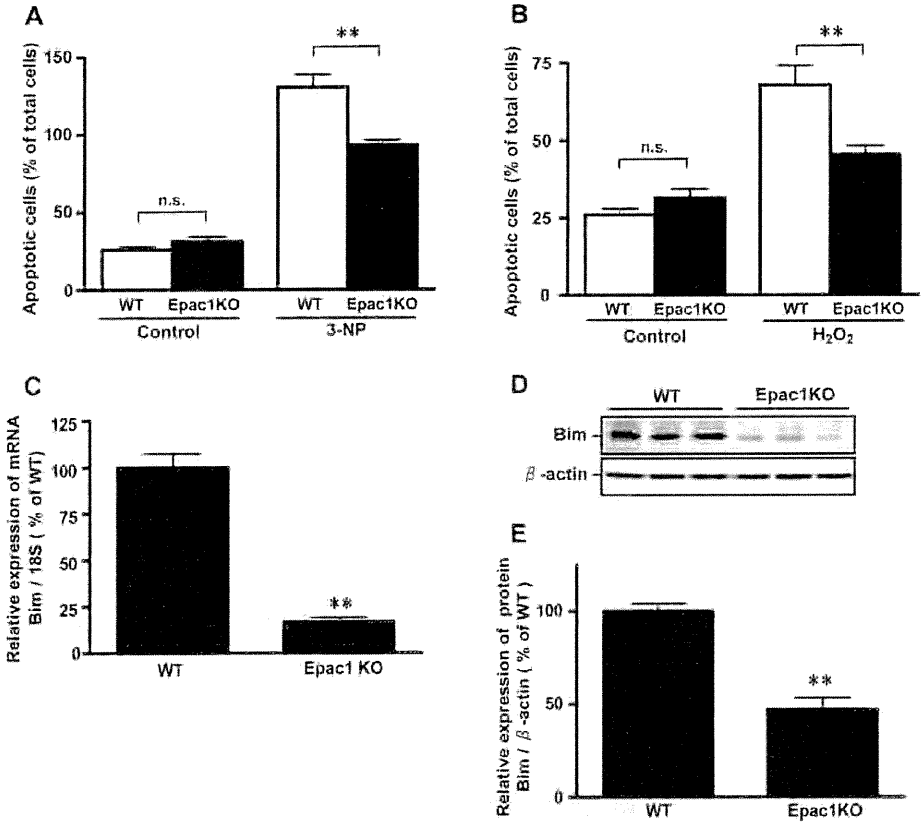

FIGURE 8. **The effect of 3-NP and hydroperoxide on apoptosis in cortical neurons from WT and Epac1 KO mice.** *A* and *B*, apoptosis was evaluated by means of TUNEL staining 48 h after the addition of the indicated reagents in cortical neurons from WT and Epac1 KO mice. The results are presented as percentages of the total cell number. *C*, the expression of endogenous Bim mRNA in cortical neurons from WT and Epac 1KO mice was quantified using real-time RT-PCR. The data are normalized to 18 S ribosomal RNA. $n = 6-8$; **, $p < 0.01$ *versus* WT. *D*, shown is a representative immunoblot of endogenous Bim protein expression in cortical neurons from WT and Epac1 KO mice. β-actin served as an internal control. *E*, the pixel intensity of the representative bands obtained in each experiment was calculated as described. $n = 4$; **, $p < 0.01$ *versus* WT mice. *n.s.*, not significant.

identified. In neuronal cells activation of cAMP/PKA signaling inhibited apoptosis induced by KCl in cerebella granule neurons (42) or by human immunodeficiency virus protein gp120 in the brain (43), promoting survival pathways in multiple neuronal cells (44, 45); these findings are in agreement with ours (supplemental Fig. 4). In cardiac myocytes, on the other hand, activation of cAMP signaling through such triggers as β-adrenergic receptor stimulation increased apoptosis (7, 8). In these studies the role of cAMP has been described primarily in terms of the activation of PKA.

Recently, several studies have suggested a contribution of either Epac alone or both Epac and PKA to apoptosis in restricted cell types including B-cell chronic lymphocytic leukemia (12), human leukocytes (11), immature B lymphoma cells (46), RINm5F β-cells (47), and H9c2 cells (48), showing that Epac and PKA play a protective role in apoptosis either alone and/or in concert in immune cells. However, the role of Epac in neuronal and myocardial apoptosis remains unknown despite the importance of cell death in tissues composed of post-mitotic cells. Our results show that stimulation and overexpression of Epac induces apoptosis in neurons but not in cardiac myocytes, implying that there are cell type-based differences in the effect of Epac activation on cell survival.

Epac-induced Apoptosis through Increased Bim Expression in Neuronal Cells—Our study demonstrated that Epac-induced apoptosis is mediated through the regulation of Bim, which acts on mitochondria as a pro-apoptotic factor, leading to disruption of the mitochondrial membrane potential. Bim binds to Bcl-2 and neutralizes its pro-survival function, resulting in apoptosis in multiple cell types (38, 49, 50). Bim is known to be expressed in neurons, hematopoietic cells, germ cells, lymphoid tissues, myeloid cells, and epithelial cells but not in cardiac myocytes, skeletal muscle, or neural-supporting cells, including glial, astrocytes, and oligodendrocytes (35). In agreement with these reports, our results show that Bim protein was highly expressed in primary culture of mouse cortical neurons but not in mouse cardiac myocytes. In cortical neurons we found that an Epac-selective cAMP analog increased Bim protein at the transcriptional level. When Bim was silenced, Epac-induced apoptosis was attenuated in neuronal cells. It should be noted that we were not able to exclude the possibility of off-target effects of the siRNAs because the rescue experiment that might exclude them is technically difficult. However, our results together with other data indicating that the suppression of the p38 MAPK pathway inhibits the elevation of Bim mRNA expression and Epac-induced apoptosis suggest that Epac-induced apoptosis is at least partly mediated by increased Bim expression. In fact, gene transfer of Bim to cardiac myocytes, which do not express Bim protein, induced apoptosis (supplemental Fig. 5). Taken together, the evidence strongly suggests that the expression of Bim is responsible for Epac-triggered apoptosis in neuronal cells, whereas Epac does not induce apoptosis in cardiac myocytes due to a lack of endogenous Bim expression. Further investigation is needed to identify the precise mechanism of Epac-induced transcriptional regulation of Bim in neuronal cells.

Changes in Epac Expression in Pathological/Physiological Conditions—Recent studies have indicated that the expression profile of Epac is altered during chronic degenerative inflammatory diseases. Epac1 mRNA, but not Epac2 mRNA, was increased in a mouse vascular injury model and was decreased in cardiac fibroblasts activated by transforming growth factor β (17, 23). Studies have reported the up-regulation of Epac1 mRNA and down-regulation of Epac2 mRNA in Alzheimer disease (13) and the up-regulation of Epac1 protein expression in inflamed rat neurons (14). These stud-

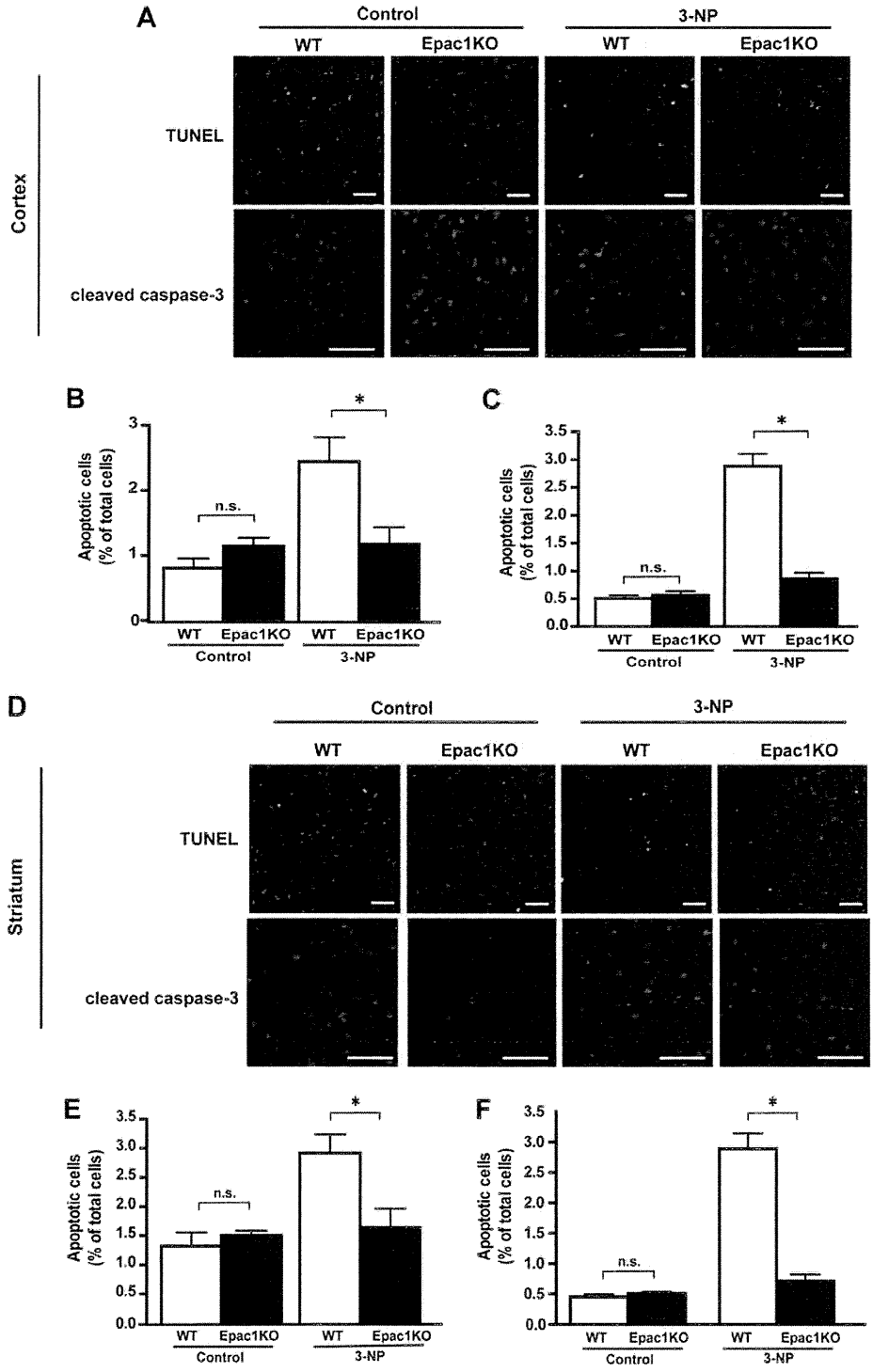

FIGURE 9. **Deletion of Epac1 suppressed 3-NP-induced brain cell apoptosis *in vivo*.** *A* and *D*, representative images of TUNEL staining and immunohistochemistry of cleaved caspase 3 of cortical and striatal sections from WT or Epac1 KO mice 24 h after injection of 3-NP. *Scale bar*, 100 μm. *B* and *E*, TUNEL-positive cells were quantified by counting nuclei in five randomly chosen fields. *C* and *F*, cleaved caspase 3-positive cells were quantified by counting nuclei in 5 randomly chosen fields. Deletion of Epac abrogated 3-NP-induced apoptosis in both the cortex and the striatum *in vivo*. The results are presented as percentages of the total cell number. $n = 5$ from 2 independent experiments. *, $p < 0.05$. *n.s.*, not significant.

ies indicate that the stoichiometry of Epac and especially that of Epac1 can be changed and selectively activated in disease conditions including neurodegenerative disorders.

Approximately half of all neurons in the nervous system undergo apoptosis during embryonic and early postnatal development (51), a period when Epac1 is highly expressed in the brain (15). Our results indicate that Epac1-induced neuronal apoptosis may be involved in the mechanisms underlying neuronal development. Nevertheless, Epac1 KO mice showed normal development up to at least 12 months of age, although no detailed assessment of their behavior, cognition, or learning memory has been made. Further studies using Epac2 KO mice and Epac1 and Epac2 double KO mice will need to be conducted given our observation that overexpression of Epac2 induced neuronal apoptosis *in vitro*.

The Effect of Epac1 Deletion on Apoptosis in Vivo—The mechanisms of neurological disorders such as Alzheimer disease, Huntington disease, and Parkinson disease are thought to stem from mitochondrial dysfunction (52). 3-NP, an irreversible inhibitor of the mitochondrial enzyme succinate dehydrogenase, is often administered systemically to treat these conditions and is considered to possess unique chemical and pharmacological traits that are accordingly considered in the generation of models of mitochondrial disorders and degenerative disorders (26, 39). The mechanisms of 3-NP toxicity are also thought to involve enhanced production of reactive oxygen species, including hydrogen peroxide, which can cause oxidative damage to DNA, lipids, and proteins (53). In the present study both 3-NP and hydrogen peroxide failed to induce apoptosis in cultured cortical neurons from Epac1 KO mice, and 3-NP-induced neuronal apoptosis was abolished in Epac1 KO mice *in vivo*. In contrast, there was no difference between Epac1 KO and WT mice in terms of 3-NP-induced apoptosis. Cardiac myocytes from Epac1 KO mice did not differ in their sensitivity to cAMP analogs (supplemental Figs. 6 and 7). Although this and our previous studies show that the inhibition of Epac1 protects 3-NP-mediated neuronal apoptosis *in vivo*

and *in vitro*, the relevance of Epac2 to this phenomenon needs to be examined in future studies. A recent study has demonstrated that Epac is involved in the secretion of an amyloid precursor protein, which has been known to induce apoptosis leading to Alzheimer disease (54). Together with our data, this indicates that selective inhibition of the Epac signal may prove useful as a therapeutic strategy in treating neurodegenerative diseases.

In conclusion, Epac induces neuronal apoptosis through increased Bim expression. Because disruption of Epac1 exerts a protective effect on neuronal apoptosis *in vivo*, inhibition of Epac may be a useful tactic in the treatment of neurodegenerative diseases.

REFERENCES

1. Mattson, M. P., and Kroemer, G. (2003) *Trends Mol. Med.* **9,** 196–205
2. D'Mello, S. R., Galli, C., Ciotti, T., and Calissano, P. (1993) *Proc. Natl. Acad. Sci. U.S.A.* **90,** 10989–10993
3. Kobayashi, Y., and Shinozawa, T. (1997) *Brain Res.* **778,** 309–317
4. Parvathenani, L. K., Calandra, V., Roberts, S. B., and Posmantur, R. (2000) *Neuroreport* **11,** 2293–2297
5. Jonakait, G. M., and Ni, L. (2009) *Brain Res.* **1285,** 30–41
6. Porat, S., and Simantov, R. (1999) *Ann. N.Y. Acad. Sci.* **893,** 372–375
7. Hirotani, S., Otsu, K., Nishida, K., Higuchi, Y., Morita, T., Nakayama, H., Yamaguchi, O., Mano, T., Matsumura, Y., Ueno, H., Tada, M., and Hori, M. (2002) *Circulation* **105,** 509–515
8. Iwatsubo, K., Minamisawa, S., Tsunematsu, T., Nakagome, M., Toya, Y., Tomlinson, J. E., Umemura, S., Scarborough, R. M., Levy, D. E., and Ishikawa, Y. (2004) *J. Biol. Chem.* **279,** 40938–40945
9. Bos, J. L. (2003) *Nat. Rev. Mol. Cell Biol.* **4,** 733–738
10. Roscioni, S. S., Elzinga, C. R., and Schmidt, M. (2008) *Naunyn. Schmiedebergs Arch. Pharmacol.* **377,** 345–357
11. Grandoch, M., Bujok, V., Fleckenstein, D., Schmidt, M., Fischer, J. W., and Weber, A. A. (2009) *J. Leukoc. Biol.* **86,** 847–849
12. Tiwari, S., Felekkis, K., Moon, E. Y., Flies, A., Sherr, D. H., and Lerner, A. (2004) *Blood* **103,** 2661–2667
13. McPhee, I., Gibson, L. C., Kewney, J., Darroch, C., Stevens, P. A., Spinks, D., Cooreman, A., and MacKenzie, S. J. (2005) *Biochem. Soc. Trans.* **33,** 1330–1332
14. Wang, C., Gu, Y., Li, G. W., and Huang, L. Y. (2007) *J. Physiol.* **584,** 191–203
15. Murray, A. J., and Shewan, D. A. (2008) *Mol. Cell. Neurosci.* **38,** 578–588
16. Ulucan, C., Wang, X., Baljinnyam, E., Bai, Y., Okumura, S., Sato, M., Minamisawa, S., Hirotani, S., and Ishikawa, Y. (2007) *Am. J. Physiol. Heart Circ. Physiol.* **293,** H1662–H1672
17. Yokoyama, U., Patel, H. H., Lai, N. C., Aroonsakool, N., Roth, D. M., and Insel, P. A. (2008) *Proc. Natl. Acad. Sci. U.S.A.* **105,** 6386–6391
18. Yokoyama, U., Minamisawa, S., Quan, H., Akaike, T., Jin, M., Otsu, K., Ulucan, C., Wang, X., Baljinnyam, E., Takaoka, M., Sata, M., and Ishikawa, Y. (2008) *Am. J. Physiol. Heart Circ. Physiol.* **295,** H1547–H1555
19. Okumura, S., Kawabe, J., Yatani, A., Takagi, G., Lee, M. C., Hong, C., Liu, J., Takagi, I., Sadoshima, J., Vatner, D. E., Vatner, S. F., and Ishikawa, Y. (2003) *Circ. Res.* **93,** 364–371
20. Yamashita, N., Uchida, Y., Ohshima, T., Hirai, S., Nakamura, F., Taniguchi, M., Mikoshiba, K., Honnorat, J., Kolattukudy, P., Thomasset, N., Takei, K., Takahashi, T., and Goshima, Y. (2006) *J. Neurosci.* **26,** 13357–13362
21. Geng, Y. J., Ishikawa, Y., Vatner, D. E., Wagner, T. E., Bishop, S. P., Vatner, S. F., and Homcy, C. J. (1999) *Circ. Res.* **84,** 34–42
22. Biju, M. P., Akai, Y., Shrimanker, N., and Haase, V. H. (2005) *Am. J. Physiol. Renal Physiol.* **289,** F1217–F1226
23. Yokoyama, U., Minamisawa, S., Adachi-Akahane, S., Akaike, T., Naguro, I., Funakoshi, K., Iwamoto, M., Nakagome, M., Uemura, N., Hori, H., Yokota, S., and Ishikawa, Y. (2006) *Am. J. Physiol. Heart Circ. Physiol.* **290,** H1660–H1670
24. Ishikawa, N., Shimada, N., Munakata, Y., Watanabe, K., and Kimura, N. (1992) *J. Biol. Chem.* **267,** 14366–14372
25. Iwatsubo, K., Suzuki, S., Li, C., Tsunematsu, T., Nakamura, F., Okumura, S., Sato, M., Minamisawa, S., Toya, Y., Umemura, S., and Ishikawa, Y. (2007) *Am. J. Physiol. Cell Physiol* **293,** C1498–C1508
26. Brouillet, E., Jacquard, C., Bizat, N., and Blum, D. (2005) *J. Neurochem.* **95,** 1521–1540
27. Christensen, A. E., Selheim, F., de Rooij, J., Dremier, S., Schwede, F., Dao, K. K., Martinez, A., Maenhaut, C., Bos, J. L., Genieser, H. G., and Døskeland, S. O. (2003) *J. Biol. Chem.* **278,** 35394–35402
28. Chae, I. H., Park, K. W., Kim, H. S., and Oh, B. H. (2004) *Clin. Chim. Acta* **341,** 83–91
29. Dong, J. W., Zhu, H. F., Zhu, W. Z., Ding, H. L., Ma, T. M., and Zhou, Z. N. (2003) *Cell Res.* **13,** 385–391
30. Communal, C., and Colucci, W. S. (2005) *Arch. Mal. Coeur. Vaiss.* **98,** 236–241
31. Wang, X., Tang, X., Li, M., Marshall, J., and Mao, Z. (2005) *J. Biol. Chem.* **280,** 16705–16713
32. Puthalakath, H., and Strasser, A. (2002) *Cell Death Differ.* **9,** 505–512
33. Putcha, G. V., Moulder, K. L., Golden, J. P., Bouillet, P., Adams, J. A., Strasser, A., and Johnson, E. M. (2001) *Neuron* **29,** 615–628
34. Guo, J., Gertsberg, Z., Ozgen, N., and Steinberg, S. F. (2009) *Circ. Res.* **104,** 660–669
35. O'Reilly, L. A., Cullen, L., Visvader, J., Lindeman, G. J., Print, C., Bath, M. L., Huang, D. C., and Strasser, A. (2000) *Am. J. Pathol.* **157,** 449–461
36. Biswas, S. C., Shi, Y., Sproul, A., and Greene, L. A. (2007) *J. Biol. Chem.* **282,** 29368–29374
37. Cai, B., and Xia, Z. (2008) *Apoptosis* **13,** 803–810
38. Adams, J. M., and Cory, S. (1998) *Science* **281,** 1322–1326
39. Pandey, M., Varghese, M., Sindhu, K. M., Sreetama, S., Navneet, A. K., Mohanakumar, K. P., and Usha, R. (2008) *J. Neurochem.* **104,** 420–434
40. Hoyt, K. R., Gallagher, A. J., Hastings, T. G., and Reynolds, I. J. (1997) *Neurochem. Res.* **22,** 333–340
41. Whittemore, E. R., Loo, D. T., Watt, J. A., and Cotman, C. W. (1995) *Neuroscience* **67,** 921–932
42. Li, M., Wang, X., Meintzer, M. K., Laessig, T., Birnbaum, M. J., and Heidenreich, K. A. (2000) *Mol. Cell. Biol.* **20,** 9356–9363
43. Chun, H., Hao, W., Honghai, Z., Ning, L., Yasong, W., and Chen, D. (2009) *Brain Res.* **1257,** 75–88
44. O'Driscoll, C., Wallace, D., and Cotter, T. G. (2007) *J. Neurochem.* **103,** 860–870
45. Pugh, P. C., and Margiotta, J. F. (2006) *Mol. Cell. Neurosci.* **31,** 586–595
46. Grandoch, M., López de Jesús, M., Oude Weernink, P. A., Weber, A. A., Jakobs, K. H., and Schmidt, M. (2009) *Cell Signal* **21,** 609–621
47. Kwon, G., Pappan, K. L., Marshall, C. A., Schaffer, J. E., and McDaniel, M. L. (2004) *J. Biol. Chem.* **279,** 8938–8945
48. Kwak, H. J., Park, K. M., Choi, H. E., Chung, K. S., Lim, H. J., and Park, H. Y. (2008) *Cell. Signal.* **20,** 803–814
49. Kaufmann, T., Jost, P. J., Pellegrini, M., Puthalakath, H., Gugasyan, R., Gerondakis, S., Cretney, E., Smyth, M. J., Silke, J., Hakem, R., Bouillet, P., Mak, T. W., Dixit, V. M., and Strasser, A. (2009) *Immunity* **30,** 56–66
50. Puthalakath, H., O'Reilly, L. A., Gunn, P., Lee, L., Kelly, P. N., Huntington, N. D., Hughes, P. D., Michalak, E. M., McKimm-Breschkin, J., Motoyama, N., Gotoh, T., Akira, S., Bouillet, P., and Strasser, A. (2007) *Cell* **129,** 1337–1349
51. Oppenheim, R. W. (1991) *Annu. Rev. Neurosci.* **14,** 453–501
52. Wallace, D. C. (1999) *Science* **283,** 1482–1488
53. Mandavilli, B. S., Boldogh, I., and Van Houten, B. (2005) *Brain Res. Mol. Brain Res.* **133,** 215–223
54. Müller, T., Meyer, H. E., Egensperger, R., and Marcus, K. (2008) *Prog. Neurobiol.* **85,** 393–406
55. Zhang, L., and Insel, P. A. (2004) *J. Biol. Chem* **279,** 20858–20865